We are IntechOpen,
the world's leading publisher of
Open Access books
Built by scientists, for scientists

6,900
Open access books available

186,000
International authors and editors

200M
Downloads

Our authors are among the

154
Countries delivered to

TOP 1%
most cited scientists

12.2%
Contributors from top 500 universities

BOOK CITATION INDEX
CLARIVATE ANALYTICS
INDEXED

WEB OF SCIENCE™

Selection of our books indexed in the Book Citation Index
in Web of Science™ Core Collection (BKCI)

Interested in publishing with us?
Contact book.department@intechopen.com

4

Biomimetic Structured Porogen Freeform Fabrication System for Tissue Engineering

Jack Zhou and Lin Lu
Department of Mechanical Engineering and Mechanics
Drexel University, Philadelphia,
USA

1. Introduction

1.1 From traditional bone scaffold replacement to tissue engineering

Non-healing bone fractures are a major health concern in the United States because of a large aging population and increased occurrence of sport-related injuries. The rate of usage of bone grafting is increasing dramatically. Bone substitutes are playing a major role in repairing or replacing damaged or diseased tissues resulting from trauma, pathological degradation, congenital deformation, cancer and cosmetics [Yang, Hillas, Baez, Nokelainen and Balan, 2004; Cuckler, 2004 and Bock, Goode and Novartis, 2003]. It was reported that over 1 million bone grafts implanted annually in US and Europe [Kelly, 2000] and over 500,000 bone-grafting procedures performed annually in the United States alone [Cutter and Babak, 2006].

Two traditional ways used in bone disease treatment are autografting and allografting. The autograft, which is a section of bone taken from a patient's own body, has been used for decades to supplement host repair, while an allograft is tissue harvested from one individual and implanted into another individual of the same species, usually taken from cadaver. Bone graft provides the structural stability and natural osteogenic behavior for patients, but both autograft and allograft failed to provide the optimum therapy and they have limitations [Giannoudis, Dinopoulos and Tsiridis, 2005 and Laurencin and Ambrosio, 1999]. Autograft is expensive and the remaining tissue at the harvest site is damaged by the removal of the graft, which often leads to donor site morbidity and raises problems of restricted availability [Silber, Anderson and Duffner, 2003]. Furthermore there is limited amount of bone available for harvesting, besides that the characteristics in resorption of the graft cannot be easily predicted. Allograft often provokes an immunogenic response, can be rejected by the host and often needs autograft tissue to initiate osteogenesis. Furthermore it may transmit disease. Although these methods are successful in some aspects, shortcomings are encountered with their usage [Gadzag, Lane, Glaster and Forster, 1995]. The main problem when using those traditional treatments is the shortage of donor tissue that limits the number of people receiving bone transplantations.

To overcome the limitations, alternative methods have been developed to fabricate synthetic bone graft substituates to promote regeneration of feasible healthy bone, however till now, no method has yet provided a satisfactory solution. As a result, researchers are turning toward a promising field of tissue engineering to develop new methods of bone

regeneration. Tissue engineering is an interdisciplinary field that draws from materials science, cell biology, and biotechnology to synthesize effective strategies for repair or replacement of damaged or diseased tissues [Langer and Vacanti, 1993]. In tissue engineering, cultured cells and biomaterials can reproduce new tissues. Typically, *in vitro* bone tissue engineering uses engineered 3-D scaffolds [Mistry and Mikos, 2005], made of synthetic biodegradable polymers [Thomson, Mikos, Beahm, Satterfield, Aufdemorte and Miller, 1999] or bioceramics [de Groot, 1984; Ohgushi, Miyake and Tateishi 2003], as substrates for 3-D culture of osteoblasts or other applicable cell types.

Today's tissue engineering research and development could be done by providing a synthetic porous scaffold that mimics aspects of the body's own extra cellular matrix (ECM), onto which cells attach, migrate, proliferate and function [Freyman, Yannas and Gibson, 2001]. Usually, the donor tissue is harvested from the patient, then, the tissue is dissociated into individual cells. The cells are then seeded into a porous scaffold in a cell culture medium *in vitro*. The diseased or damaged tissue is removed and the scaffold with attached cells is implanted. Over time, the synthetic scaffold degrades into the body and the cells produce their own natural ECM [Chapekar, 2000; Freyman et al., 2001].

For bone tissue engineering, a scaffold is used to either induce formation of bone from the surrounding tissue or act as a carrier or template for implanted bone cells or other agents [Burg, Porter and Kellam, 2000]. Bone regeneration generally involves few critical components: a morphogenetic signal, host cells that will respond to the signal, a template of this signal that can deliver it to the damaged tissue then serve as a scaffold for the growth of the host cells, and a feasible, well vascularized host bed [Geiger, 2001]. Bone morphogenetic protein (BMP), a group of proteins responsible for a variety of events in embryogenesis and in postnatal skeleton, acts as the morphogenetic signal [Burg et al., 2000]. BMP causes pluripotential cells to differentiate into osteoblast, bone-generating cells. The scaffold servers as a carrier of BMP or functions as a template for implanted bone cells or other agents, and it also supports ingrowth of capillaries and cells from the host into 3-D substrate to form bone [Coelho, 2005 and Saito, 2003]. Scaffolds degrade at a controlled rate that is compatible with tissue ingrowth rate; the degradation products can be easily metabolized or excreted. At the end, a new, completely natural bone tissue is formed in the place of scaffold [Burg et al. 2000, Klawitter and Hulbert. 1971].

1.2 Required characteristics of bone scaffold

The bone scaffold must meet certain requirements. The ideal bone scaffold should be biocompatible and osteoconductive, contain osteoinductive factors to enhance new bone ingrowth, and contain osteogenic cells to begin secreting new ECM. In general, the required characteristics of bone scaffold can be classified into four related aspects:

1. *Biological properties*: The scaffold material must be biocompatible and promote cell adhesion, migration, and ingrowth. As the cells produce their own ECM, the synthetic matrix should degrade into nontoxic components that can be eliminated from the body [Freyman et al., 2001].

2. *Internal porous structure*: Both cell seeding and bone ingrowth normally are well developed with high porosity, typically among 50-90%. In general, the pore size falls within a certain critical range to promote cell seeding and ingrowth [Freyman et al, 2001 and LeGeros, Parsons, Decals, Driessen, Lee, Leu and Metger, 1988]. Both upper and lower bounds are computed by different factors. Cell size controls the lower bound while the specific surface area via the availability of binding sites decides the upper

bound. Klawitter et al's study showed that the optimal pore size for bone ingrowth is in the range of 100-250 μm [Klawitter et al., 1971]. Cell ingrowth and nutrient transport are interconnected with the porosities.

3. *Mechanical properties*: The primary bone tissue has relatively high compressive strength that supports the body weight. So the scaffold must provide mechanical support during the reconstruction process. Mechanical integrity for the scaffold design has to be sufficient to resist handling during implantation and *in vivo* loading. An ideal scaffold should be biomechanically similar to the type of bone being replaced in order to function quickly as a synthetic bone replacement. In general, the compressive modulus is in the range of 0.01 to 2.0 GPa for trabecular bone, and 14 to 18 GPa for cortical bone [Athanasiou, Zhu and Wang, 2000]. The scaffold should be able to maintain sufficient mechanical properties until newly formed bone can assume a structural role and then the scaffold can be degraded and resorbed in the process of bone regeneration. Numerous studies have demonstrated profound effects of mechanical forces on cells using *in vivo* and *in vitro* models. Chen, Yannas and Spector [1995] found that the mechanical properties of the substrate are significant factors affecting biological response, as the mechanical environment of the contained cell is determined by these properties.

4. *Precise three-dimensional shape*: The scaffold must be manufactured to an arbitrary complex 3-D shape which can match that of the tissue to be replaced, at both the microscopic and macroscopic levels.

1.3 Current needs in tissue scaffold manufacturing

From the perspective of length scale, bone has a complex varied hierarchical structure and is mainly classified into two types at the macrostructure level: cortical bone (or compact bone) and cancellous bone (or trabecular bone). At the microstructure level, in the scale of 10 to 500μm, there are Haversian systems, osteons and single trabeculae; and in the scale of 1 to 10μm there are sub-microstructure lamellae. Fibrilar collagen and embedded mineral are the nano-structural components at the scale of a few hundred nanometers to 1μm. Subnanostructures with size below a few hundred nanometers consist of molecular structure of constituent elements such as mineral, collagen, and non-collagenous organic proteins [Rho, Liisa and Zioupos, 1998; Mehta, 1995; Weiner and Traub, 1992 and Weiner and Wagner, 1998]. Figure 1 illustrates the basic architecture of the bone [Rho et al., 1998]. The collagen fibers run parallel to each other to form laminae or lamellae. The lamellae can be arranged in concentric cylindrical layers in osteons, or parallel in the interstitial lamellae, outer circumferential lamellae or inner circumferential lamellae. Haversian systems and osteons constitute the main portion of compact bone, originated from a process of erosion initiated from the vascular channel towards the periphery and followed by a later centripetal deposition of concentric lamellar bone. Osteons are surrounded by a cement line as the result of bone resorption. The vascular channel of the center of the osteon is called a Haversian channel, and its diameter varies depending on the amount of lamellar bone deposited. Different osteons are mutually connected by radially oriented Volkmann channels. Blood vessels run inside the Haversian and Volkmann channels [Rho et al., 1998; Mehta, 1995; Weiner et al., 1992 and 1998].

The various scale structures perform various functions, i.e., mechanical, biological and chemical. In bone tissue engineering, the scaffold with biomimetic microstructures can be made in different bone types, such as trabecular or compact bone, however the structures at

sub-micron and even smaller scales are the results of human body's biological and chemical processing, and we don't need and also cannot fabricate them. The artificial scaffold acts only as temporary ECM, and will be resorbed and remodeled by biological and chemical processes of human body to achieve completely natural bone tissue at the end of the recovery. Since the high mechanical strength requirement for artificial cortical bone is difficult to reach from most biomaterials, our target tissue in this research will be the highly porous lower-strength trabecular bone.
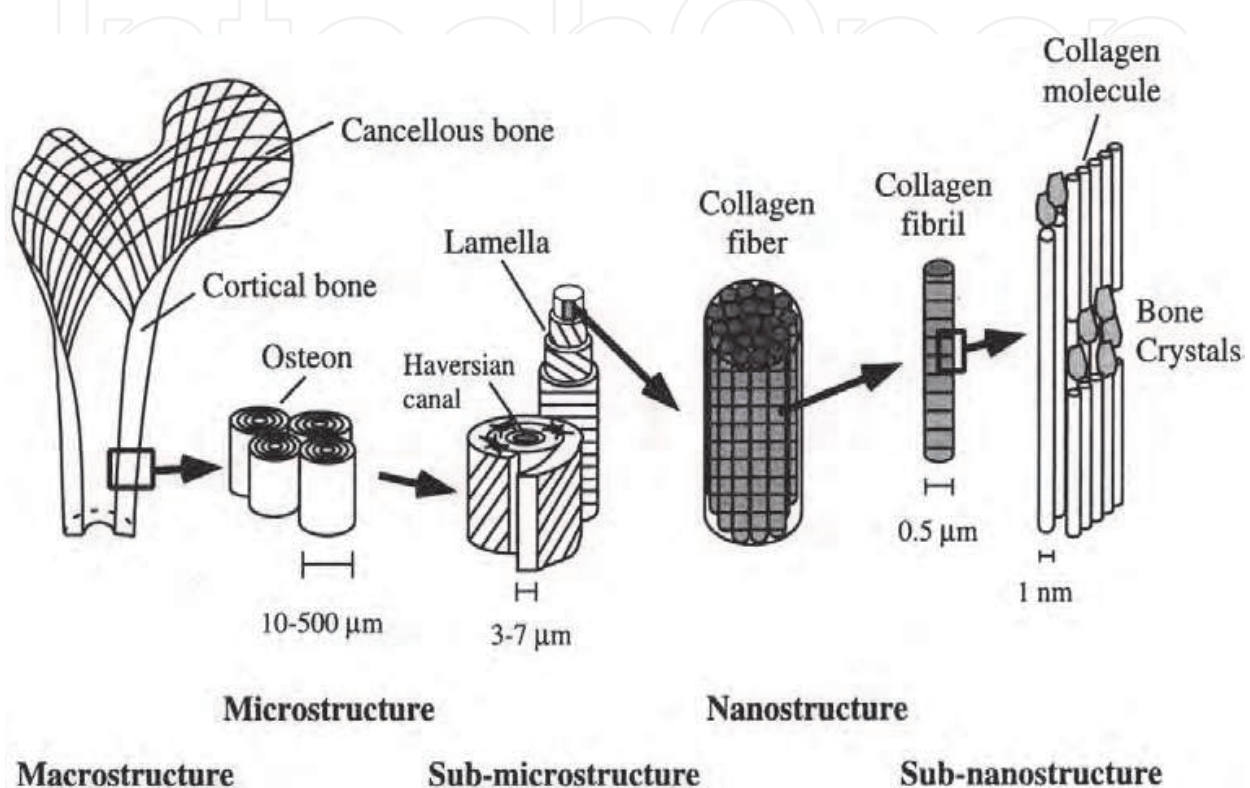
Fig. 1. Basic architecture of bone [Rho et al., 1998].

Since the porosity of the bone scaffold is very important, many manufacturing techniques and biomaterials were used to control the pore size and porosity rate. New biocompatible materials and a number of fabrication technologies have been explored and developed to create synthetic bone grafts, which process biodegradable and biocompatible materials into a 3-D scaffold with high porosity and surface area [Hutmacher, 2000]. These technologies include Porogen Leaching, Fiber Bonding, Gas Foaming, Gel Casting, Solution Casting and Emulsion Freeze-Drying [Gadzag et al., 1995; Chapekar, 2000; Mikos, Bao, Cima, Ingber and Vacanti, 1993; Harris, Kim and Mooney, 1998; Coombes and Heckman, 1992; Singhal, Agrawal and Athannasiou, 1996 and Mooney, Baldwin, Suh, Vacanti and Langer, 1996]. In the above mentioned methods, although researchers have achieved significant progresses in making a porous scaffold for bone tissue engineering, many difficulties remain. Most of the above-mentioned methods for fabricating 3D scaffolds are mainly used for laboratory testing purpose and are not practical production process, placing substantial limitations on manufacturing. Consequently, the control of scaffold architecture, such as pore size, shape, porosity, and interconnectivity is hard to reach, thus using these fabrication techniques is still highly process driven, not design driven [Lee, Ryu, Lee, Hong, Chang and Lee, 2005]. And most of the above-mentioned processes involve organic solvent or high temperature

melting and sintering, which may denature bioactive factors such as BMP. In most methods, an internal porous structure generated by randomly packed porogen cannot be controlled precisely and flexibly. For example, the pore size and porosity at different sections of the scaffold should be different in many cases, and all the pores should be interconnected; however, these requirements cannot be obtained or guaranteed. Furthermore, most of the scaffolds/organs made through these processes have relatively low mechanical strength, which may lead to problems with implant failure and stress overloading. It is hard for the above mentioned techniques to produce the functional structure with defined morphology which is important for the regenerative tissue. A current limitation of commercializing scaffolds for bone repair is the lack of a manufacturing system capable of producing defined structures with a high degree of reproducibility [Gadzag et al., 1995 and Chapekar, 2000].

Solid freeform fabrication (SFF), also known as rapid prototyping (RP), is a new manufacturing technology that is capable of producing complex freeform parts directly from a computer aided design (CAD) model of an object. Recently, SFF has been used in direct fabrication of porous scaffold for tissue engineering [Geng, Feng, Hutmacher, Wong, Loh, Fuh, 2005; Taboas, Maddox, Krebsbach, and Hollister, 2003; Williams, Adewunmi, Schek, Flanagan, Krebsbach and Feinberg, 2005; Hollister and Maddox, 2002]. However SFF techniques still present various problems in materials, processing methods, and bionic requirements when making bone scaffolds. The main difficulty is to make highly porous parts with delicate internal structure, sufficient mechanical strength, and integrity. Some commonly used bone making materials, such as Hydroxyapatite (HA) and Calcium Phosphate Cement (CPC) are difficult to use directly with SFF methods, due to their low fluidity, poor manufacturability, high processing temperature and long degradation time. In addition the usage of SFF to manufacturing scaffolds for tissue engineering is limited by the fact that SFF machines must be adapted to the fluid mechanical properties of each biomaterial under consideration. In most of SFF methods, the machine parameters must match the physical properties of the build material, such as melting temperature, viscosity and surface tension. These properties vary greatly amongst different biomaterials, precluding the use of a single machine for direct fabrication of scaffolds from multiple biomaterials, requiring more complicated multi-nozzle designs. Therefore, it is desirable to develop SFF fabrication processes in which a single, universal porogen material is used to build porogens (a negative pattern of bone and bone ECM) that may then be injected with a wide range of biomaterials.

There were few researchers that have worked on porous scaffold manufacturing in the last decade using so called porogen method [Gadzag et al., 1995; Harris et al., 1998; Coombes and Heckman, 1992 and Mooney et al., 1996]. Most of them just used simple molds and injected with biomaterial, then used salt leaching, gel casting or gas forming to create randomly packed pores. To distinguish with other researchers previously mentioned, our proposed method uses SFF technique to fabricate structured porogen. The structured porogen can be precisely designed by directly reconstructing CT and MRI images or CAD model. Then the structured porogen with negtive complicated external shape and interconnected internal structure can be manufactured using SFF techniques. Following the fabrication of the porogen, the biomaterials can be injected. After removal of the porogen, the scaffolds can be made. This proposed study can overcome the existing limitations and fabricate desired bone scaffolds, by combining the advantages of SFF method, structured porogen design, and reverse injection of bioactive composite materials to establish an innovative bone and tissue manufacturing system.

1.4 Proposed structured porogen mold method and its technical advantages

Briefly, the structured porogen mold bone fabrication method (Figure 2) consists of four steps. 1) Based on multi-planar images obtained from computed tomography (CT) or magnetic resonance imaging (MRI), a 3-D CAD model of bone tissue can be reconstructed. 2) Based on the CAD model of bone structure, a structured porogen can be designed and fabricated using SFF technology in stacking biocompatible sucrose or other materials. 3) A melted PCL (or other biopolymer) and CaP composite or liquid-like gel of calcium phosphate cement is then injected into the negative skeleton to form the desired bone scaffold. 4) The negative skeleton is removed by immersing the assembly of the composite and skeleton into suitable solvent, and then the skeleton is dissolved, leaving the bone scaffold.

The porogen mold bone tissue fabrication method has the following uniqueness and advantages:

1. Comparing with traditional bone treatments, our structured porogen method is more convenient to use, which allows for the use of a single building material in the SFF machine to fabricate multiple biomaterial scaffolds without recalibrating the SFF machine.

2. Up to now, mechanical strength is a major drawback of artificial bone scaffold. The use of composites to improve the scaffold strength has been studied and recognized. By using composite materials, the composition of the composite scaffold can be adjusted to fit different requirements such as biodegradation rate and mechanical strength. In this research, composites of ceramics and polymer are selected as filling materials. Therefore the mechanical properties can be improved.

3. The precise shape of the bone substitute scaffold is reconstructed through reverse engineering based on the CT or MRI images. The unique manufacturing capability of SFF enables us to make the negative skeleton with both the external shape and internal porous structure of the bone scaffold accurately, including spatial gradients in microstructure.

4. The bone scaffold is required to be of high porosity. Such high porosity is very difficult to achieve by using SFF technology directly, because the fabricated part must have a solid-to-void ratio less than 10%, and the built porous structure cannot hold shape. Conversely, it is much easier to make an inverse-porous structure with the solid-to-void ratio of over 90%, in other words, to make the porogen of ECM. In this study, the porogen of bone ECM will be fabricated first, then the CPC and biopolymer composite will be injected into the interconnected cavities to form the scaffold, and then the negative pattern will be removed to create porous structure (Figure 3).

5. In addition, by using of the structured porogen method the resolution of our fabricated scaffolds can be improved 2 to 4 folds compared to directly built method in use of same SFF machine.

In this study, PCL and Calcium Phosphate (CaP) were chosen as the injective biomaterials. The innate rigidity of PCL makes this material well suited for the fabrication of tissue engineering scaffolds, mainly for orthopedic applications [Shin, Yoshimoto and Vacanti, 2004; Chen, Bei and Wang, 2000 and Rohner, Hutmacher, Cheng, Oberholzer and Hammer, 2003]. PCL was attractive also due to its low cost and sustained biodegradability although it is not bioactive [Kim, Knowles and Kim, 2003]. Calcium phosphate, a major constituent of native extracellular matrix in bone, has been widely used as a bone substitute or as coatings on metal implants in orthopedic and dental applications to accelerate bone reconstruction or
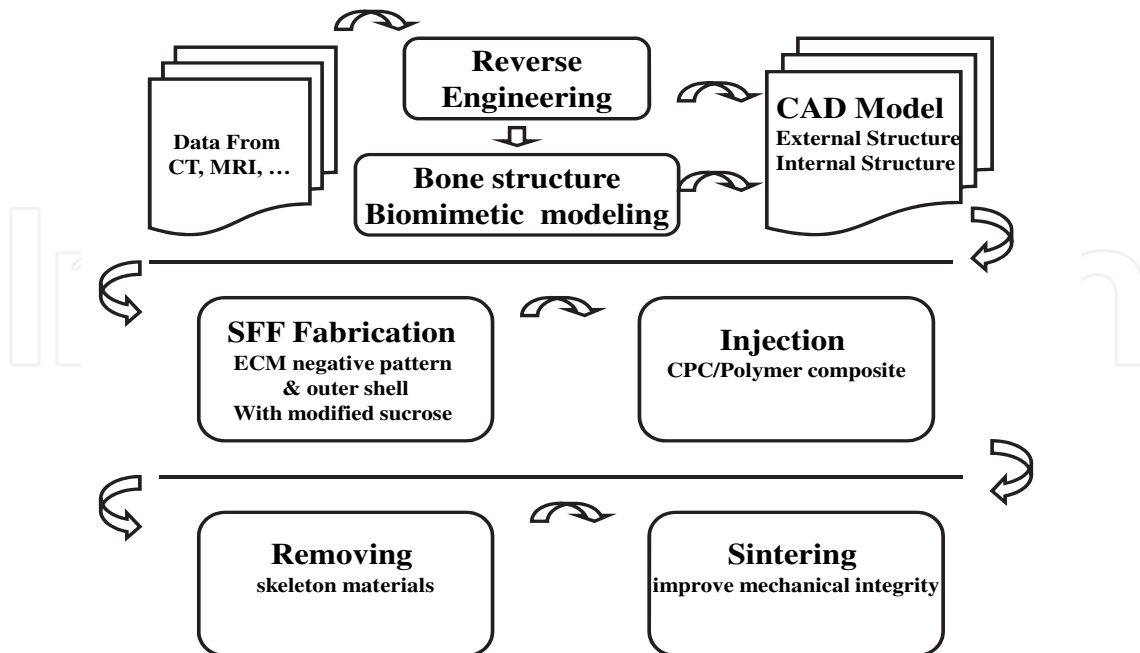
Fig. 2. Diagram of the main processes in the bone scaffold and tissue manufacturing system.

(A)   (B)   (C)
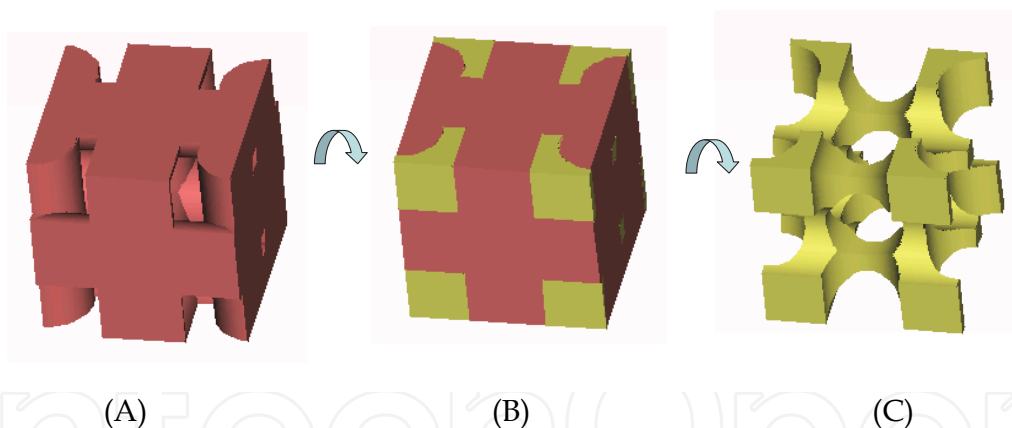
Fig. 3. A simplified illustration of structured porogen method for bone scaffold fabrication (note: for easy illustration a square shape is used): (a) structured porogen takes the majority of the volume; (b) biopolymer composite injected into the skeleton cavity; (c) after removing the porogen a thin wall fine structure scaffold is formed.

skeletal fixation [Albee, 1920; Ruhe, Hedberg, Padron, Spauwen, Jansen and Mikos, 2003; Xu and Simon, 2004; Xu, Quinn, Takagi and Chow, 2004and Barralet, Grover, Gaunt, Wright and Gibson, 2002]. CaP is bioactive, so the osteoblasts can successfully attach with biological hard tissue. However, because it has relatively poor mechanical properties (it is a brittle material) CaP is not suitable for load-bearing sites or large bony defects. Incorporation of CaP into PCL would overcome the shortcoming of hydrophobicity of the PCL and the brittleness of the ceramic CaP. In our research CaP microparticles will be hybridized with PCL melting solution to make the PCL-CaP composite scaffolds. With alteration in the

CaP/PCL ratio, the morphology, mechanical properties, and biodegradation behavior were investigated. This process is able to design a bone scaffold that has the exact shape and similar internal structure of the bone tissue, and sufficient mechanical strength.

2. Structured porogen method for bone scaffold fabrication using drop on demand RP machine

At present, SFF is the best way to generate defined porous structures. SFF technology combined with 3D reconstruction based on CT and MRI data is able to form high precision, realistic models. The use of SFF technology to manufacture scaffolds for tissue engineering applications is limited by the fact that SFF machines must be calibrated for each material used. The machine parameters must match the physical properties of the building material. These properties vary greatly in biomaterials, making the use of a single machine for fabrication with multiple biomaterials difficult. The structured porogen-based bone fabrication method allows for the use of a single building material in the SFF machine and the flexibility to use any biomaterial or composite that can be injection molded. In addition, the use of a porogen allows for the fabrication of structures with much fine features compared with direct building method.

2.1 Introduction of drop on demand RP machine

In this part of study a commercial drop on demand RP machine (Solidscape Model Maker II) that uses thermal phase change ink jetting technology has been used to test our structured porogen method for bone scaffolds fabrication. Figure 4 shows a schematic view of Solidscape machine (Merrimack, NH). This technology deposits melted build material onto substrate which cools to form solid on impact. 3-D CAD design first was converted to STL representation. Then it can be imported into Solidscape's ModelWorks control software for orientation and build configuration selection. ModelWorks then automatically slices the STL file and converts it to a binary file to drive the nozzles. There are two moveable inkjet heads (Figure 5 A), both depositing a kind of material. One head deposits a green thermoplastic build material - similar to wax. The other deposits a red wax that serves as a sacrificial support material for the support of undercuts and overhanging features and is easyly dissolved in a solvent after the model is complete. These materials are solid at room temperature, but they are stored in a molten liquid state at an elevated temperature in reservoirs which are located at the back of the system, and fed to the individual jetting heads through thermally insulated tubing. The inkjet heads deposit micro-droplets of the materials as they are moved side to side on the build platform following the cross-section geometry to form a layer of the model. The inkjet heads are controlled and only deposit droplets where they are needed. The materials solidify due to rapid drop in temperature after they are printed. After an entire layer has been formed, a milling head is passed over the layer in making it a uniform thickness assuring great precision. The excess material is collected by a vacuum system and captured in a filter. The build platform is then moved down a layer thickness and the subsequent layers built in the same manner. The operation of the nozzles is checked after each layer has been finished by printing a line of each material on a drum and reading the result optically. If all goes well, the building table is moved down a layer thickness and the next layer is begun. If a clog is detected, a jet cleaning process is performed. If the clog is cleared, the problematic layer is cut off and then reprinted. It gives us the ability to correct mistakes resulting from a failure of the inkjet. When the model is finished, the wax support material is either melted or dissolved away.
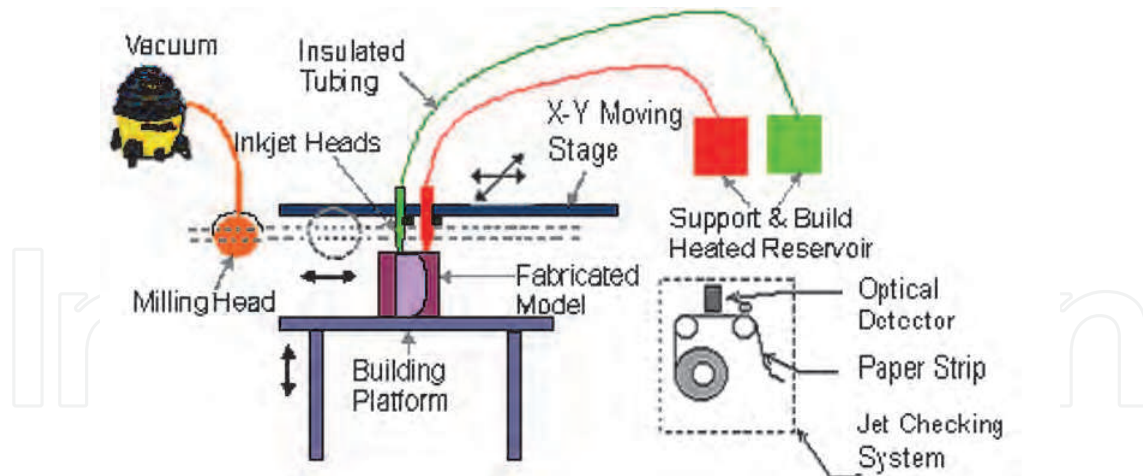
Fig. 4. Schematic view of Solidscape system.
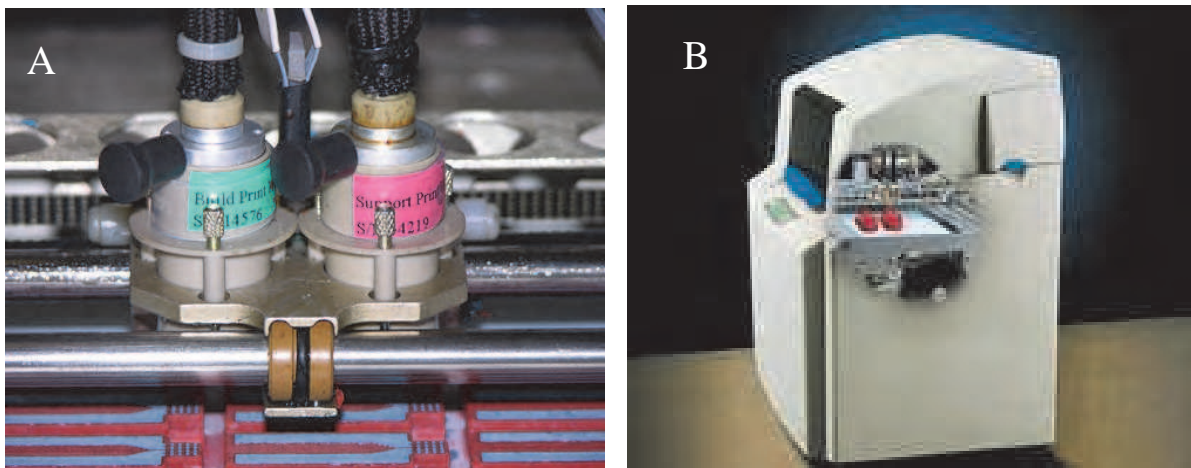
Fig. 5. Digital photograph of (A) Inkjet print heads; (B) Solidscape Modelmaker II RP machine.

2.2 Porogen design and fabrication
2.2.1 CAD designs of porogen

Pro/E software package was used to design porogens and then transfer the design into STL format which is required by Modelwork software to run the RP machine. In order to simulate the global pore structure present in bone tissue, those porogens were designed with fully interconnected voids. They had different design with different size, varying porosity and internal architectures. Figure 6 (A) shows a fabricated porogen design, its CAD model is shown in Figure 6 (B). Figure 6 (B) to (F) are all possible porogen designs. After fabrication and injection tests, considering the uniformity and ease in making the porogens we finalized our design which is shown in Figure 6 (C). In this design, each void of the square scaffold is in the shape of a cube and is separated from adjacent voids by struts on four of its sides. Hence the resulting structure of the scaffold was a series of rods with rectangular cross-sections connected to one another. The dimensions of the voids and the rod cross sections were equal and constant throughout the scaffold volume. The overall scaffold volume was cube in shape that is easy for the machine to make. Scaffold designs were created for a constant pore size of 600μm, 400μm, 300μm, and 200μm in squware sides.

In order to minimize air entrapment and weld line formation, the porogen was designed such that molten biomaterial would flow into the cavities of the porogen through a single injection gate (Figure 7B). The dimensions of the gate's cross-section were equal to the pore size of the particular scaffold being injected (e.g. the gate was 600×600 μm^2 for 600 µm-wide pores), except for the fabrication of 200 µm pore scaffolds, which required an opening of 250×250 μm^2. Therefore, a transition region was needed to go from a relatively large basin where molten material could be deposited down to the gate dimension corresponding to the desired pore size of the scaffold being fabricated (Figure 7B). The interior diameter of the basin was designed such that the plunger of a standard plastic 1ml syringe could be used to force the molten biomaterial into the cavities of the porogen (Figure 7A). By using a syringe, a pressure could be applied to the scaffold material to help overcome the frictional forces resisting material flow through the porogen. To accommodate using a syringe for injection, one end of the porogen had a basin and a hole through the wall of the porogen. The basin allows a flow front of the material being injected to develop in a direction parallel to the porogen surface containing voids. As a result, the scaffold material begins filling the first row of voids at approximately the same time. Therefore, the porogen fills more uniformly and the time required to fill the porogen is reduced. A cutout view model of the desired resultant scaffold geometry following porogen injection and subsequent removal is shown in Figure 7C. In order to empirically determine the minimum porogen basin wall thickness and maximum biomaterial injection temperature for which thermoplastic porogens would consistently maintain structural integrity, simple destructive testing was conducted. Based on these preliminary experiments, a 3.18mm wall thickness and a biomaterial injection temperature of 72 °C were selected. Then the designed porogen was imported to the Modelwork software and sliced with the setting layer thickness of 38.1 µm. Following the same procedures mentioned before, the porogens were fabricated.
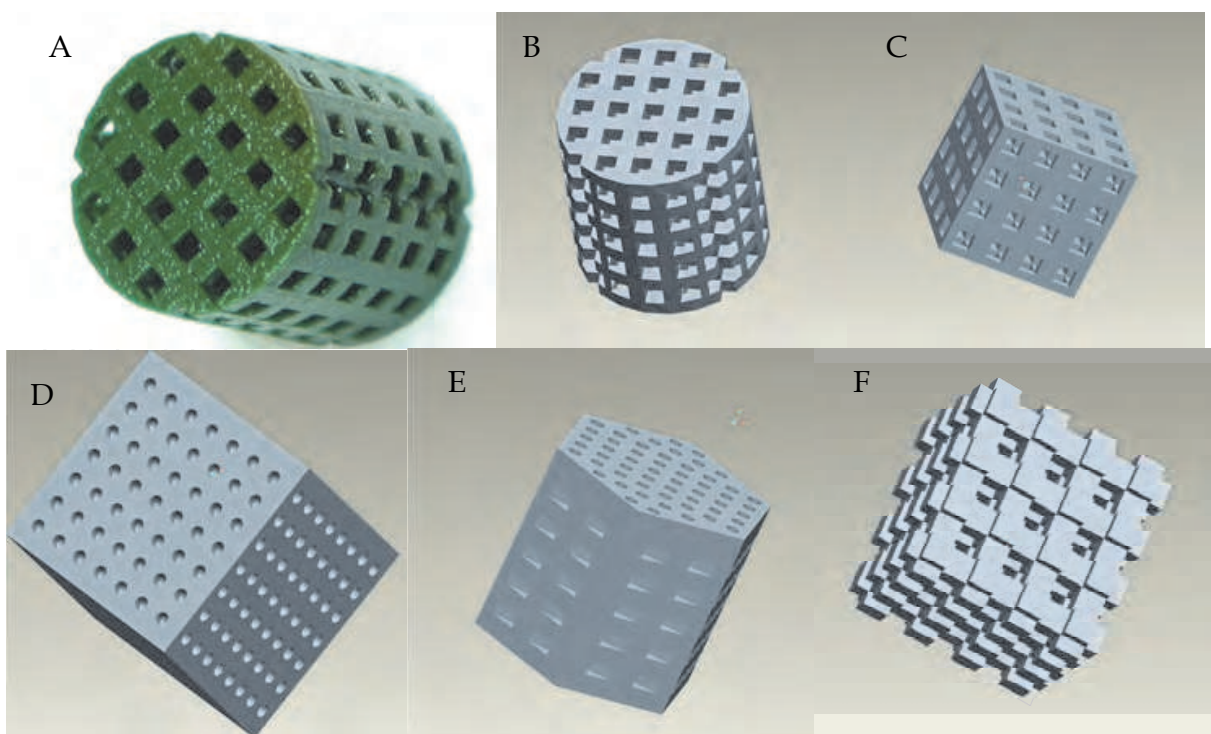

Fig. 6. CAD models of designed porogen.

2.2.2 Scaffold fabrication using structured porogen method

In previous studies, generation of biocompatible scaffolds using injectable porogens has been accomplished by polymer solution casting [Taboas et al., 2003; Ren, Ren, Zhao, Huang and Pan, 2007]. However, most of the solvents which are commonly used to solubilize synthetic biopolymers, such as dimethyl formamide (DMF), chloroform, and dioxane, are highly cytotoxic and will also dissolve the proprietary thermoplastic material used with the Solidscape machine, making solution casting difficult to implement in our process. Therefore, in order to use the parts fabricated by the machine without any secondary processing, we chose to inject molten biopolymers into the porogen.

After the fabrication of structured thermoplastic porogens, scaffolds were generated by injection molding as described below. The overall process is illustrated in Figure 7A. The fabrication process for three biomaterials (PCL, CaP and CPC), as well as their composites (PCL/CaP) has been developed and tested using the thermoplastic porogen system. The resultant scaffolds demonstrate the defined porous structure designed into the thermoplastic porogens (Figure 7E). These scaffolds demonstrate an interconnected porous structure that might be suitable for tissue engineering applications.

2.2.2.1 PCL scaffolds fabrication

PCL pellets were melted in an oven (VWR 1410) at 72°C. Concomitantly, the porogens were also preheated to 72°C. Heating of the porogens prior to injection with PCL allowed for complete penetration throughout the porogen structure. Attempts were also made at filling unheated porogens. The depth at which the PCL injected into the porogen was a function of pore size and temperature of molten PCL. In unheated porogens the molten PCL solidified in the voids before reaching the other end of the porogen. The smallest pore size in unheated porogens which allowed 72°C molten PCL to reach the opposite end of the porogen was 600μm. For smaller pore sizes, the molten PCL solidified in the pores before reaching the other end of the porogen. Fill tests were also conducted for various temperatures of PCL while the porogen temperature was held at room temperature. During heating the PCL was occasionally mechanically agitated by hand and visually inspected for solid particles. A half hour prior to scheduled injection, the molten PCL was subjected to a vacuum in order to minimize air bubbles in the scaffolds. Molten PCL was drawn into a 1 ml syringe (Fisher Scientific). The flat tip of the syringe was placed into the basin, thus allowing the plunger to advance from the syringe body into the cylindrical basin of the porogen (Figure 7A). The syringe was emptied quickly and the filled porogen was allowed to cool to room temperature. After solidifying, excess PCL was trimmed using razor blade.

A number of reagents and techniques were used to separate the thermoplastic porogen material from the biomaterial scaffolds after biomaterial solidification, after series of tests, ethanol was selected and used through the remainder of this part of study. First the injected porogens were immersed into 99% ethanol (Fisher Scientific) in a 50ml test tube. The ethanol in the tube was removed and replenished with new ethanol for a minimum of three times. The tube was shaken vigorously and the solvent replaced every 3-5 minutes, until all porogen material was dissolved, as evaluated by the colorless appearance of the solvent. Using this method, most of the porogen material was removed in 10 min, with soaking for no more than 1 h to remove residual thermoplastic from the scaffold center. After porogen removal, the scaffolds were then allowed to air-dry at room temperature and stored dry as long as needed prior to cell culture and mechanical testing. A cut-out view of the scaffold structure corresponding to the porogen design is shown in Figure 7C. PCL scaffolds with a void size of 200μm (Figure 8 A & B), 300μm, 400μm, and 600μm (Figure 8 C), were successfully fabricated.
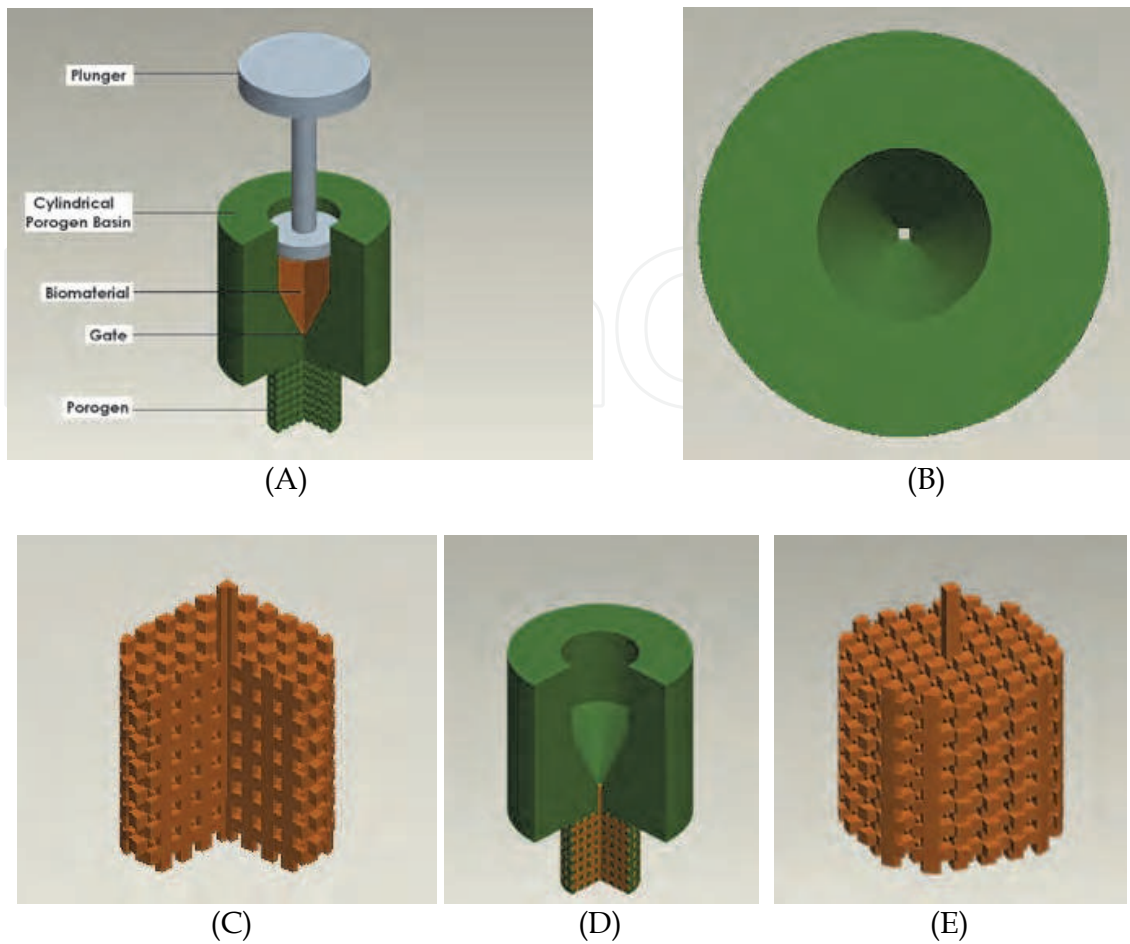
Fig. 7. Computer generated models of the porogen illustrating key features of the injection molding process. A: Injectable porogen with cylindrical basin for loading molten biomaterial that is injected through the single injection gate using a syringe plunger; B: Overhead view shows the single injection gate equal to the largest sized feature in the porogen (250, 300, 400 or 600 µm); C: Cut-out view of resultant scaffold; D: Molten biomaterial injection; E: Theoretical model of resultant scaffold consisting of pores with the void volume corresponding to the porogen gate dimension (250 - 600 µm).
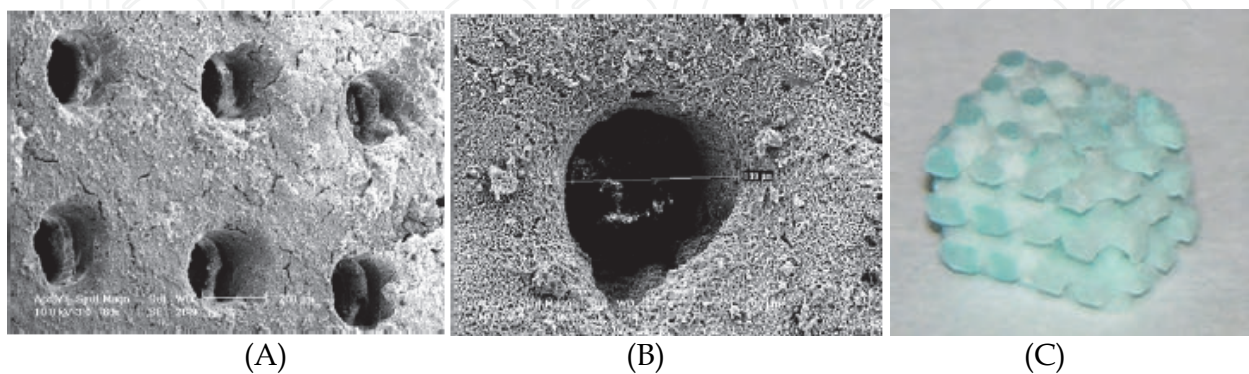
Fig. 8. SEM micrograph of (A) 200 micron pores in an injection molded PCL scaffold (B) single pore ~ 200 micron. (C) Digital photograph of 90/10 PCL-CaP scaffold (size: 4.2×4.2×5.4mm, pore: 600 µm).

2.2.2.2 PCL-CaP composite scaffolds fabrication

PCL-CaP composite scaffolds were fabricated in the same fashion as the PCL scaffolds, with the additional step of preparing the PCL-CaP composite. For that, dry PCL pellets and CaP, calcium phosphate tribasic, powders (Fisher Scientific) were weighed using a standard balance (VWR) and mixed at the desired ratios in beaker. After melting at 72°C, the mixture was homogenized using an ultrasonic probe, and reheated as necessary; total mixing time was approximately 30 minutes. Scaffolds were made with ratios (w/w) of 90% PCL to 10% CaP (Figure 8C) and 80% PLC to 20 % CaP. PCL-CaP composite scaffolds with a void size of 600 and 400μm were successfully fabricated.

2.3 Porosity and voids analysis using micro CT

Since the porosity is very critical to bone ingrowth, nutration and waste transport, nine scaffolds with 600μm pores made of pure PCL, 90/10 and 80/20 PCL–CaP (n≥3 for each material) were scanned using a SkyScan 1072 Microtomograph (μCT) scanner (Micro Photonics) to evaluate the porosity of fabricated scaffolds. This is a compact, desktop X-ray system for non-destructive 3-D microscopy with 5μm resolution and 2μm detectability operating at 100 kV, yielding transmission images which can be used to reconstruct cross sections or the complete 3-D internal microstructure. The image pixel size was set at 6.1μm in this study. The output format for each specimen was 976 serial 1024×1024 bitmap images. These slice images were viewed in SkyScan's TView software and reconstructed by CT Analyzer software.

By selecting darker thresholds, the struts of a specimen may be reconstructed. Conversely, by selecting the white levels of the bitmap images, the pores in the specimen can be visualized. Thresholds of the gray scale images were inverted to allow measurement of the volume of all pore spaces. The ratio of pore volume to total volume was then calculated to determine the porosity. μCT analysis based views of an 80/20 PCL–CaP composite scaffold fabricated using a 600μm porogen are shown in Figure 9. Pore corners in the horizontal build plane ($x–y$ directions) were quite sharp (Figure 9 A and B), whereas rounding of the scaffold pore corners was observed in the vertical build plane (z-axis, Figure 9 C). The porosity of our 600μm scaffolds was determined for each of the materials by volumetric analysis of 3-D reconstructions from μCT data (see Figure 10). For the 600μm scaffolds, the theoretical porosity based on the porogen design was 59.9%, while measured values were 52.6% for pure PCL, 57.2% and 58.2% for 90/10 and 80/20 PCL–CaP composites, respectively. These data conform fairly well (within< 5% for 90/10 and 80/20 PCL–CaP) to the theoretically calculated porosity. The somewhat higher porosities observed for the PCL–CaP composites vs. pure PCL may be due to resistance to flow within the porogen caused by the solid CaP particles, whereas the pure PCL melt flows more freely during injection molding, thus more completely filling and compressing the porogen. From Figure 10, we can also see that increasing the CaP to PCL ratio made the scaffolds rough due to the large amount of CaP particles.

2.4 Mechanical testing

Mechanical properties such as compressive strength, tensile strength and elastic modulus of the scaffolds is critical to bone scaffolds and they are also a weak point of most biomaterial artificial scaffolds. To find out the mechanical integraty of our structured porogen method

fabricated scaffolds, we have conducted a series of mechanical testings on our composited materials as well as the scaffolds.

2.4.1 Compression test for bulk PCL-Cap composite materials and scaffolds

Compression tests of solid rods made of PCL and PCL-CaP composite were performed for specifying the properties of the composite as well as validating the properties of pure PCL, on an Instron 5543 uniaxial testing system using 1KN load cell. 1cc disposable syringes were used to make the testing specimens. First the degassed molten PCL and PCL-CaP composite materials were drawn into the syringe. Then filled syringe was solidified at room temperature. The two ends of the syringe were cut and the center part was left and cut to certain length (15.24 mm, D=4.8mm). Five specimens of each material were tested according to the guidelines specified in ASTM D695-02a. In addition, compression testing was done on 600µm pore pure PCL, 90/10 and 80/20 of PCL-CaP scaffolds (n=6) at a compression rate of 1mm/min using the same system described above with a 100N load cell and compression to failure. Effective stress was computed based on the scaffold cross-sectional area. The ultimate compressive strength (UCS) as well as the compression modulus (CM) was calculated from the effective stress-strain diagrams. And the average UCS and CM are plotted as a function of composition.

As seen in Figure 11 the increase in CaP content of the composite significantly raised the CM and UCS as well as stiffness of the material of the samples ($P<0.002$). This is particularly advantageous for making scaffolds for application in hard tissue engineering. But as the fraction of the composite increases the structure becomes brittle. Scaffold stress–strain curves show multiple failure points due to failure of the weakest strut, prior to collapse of the entire scaffold structure (Figure 3.29). In order to assess potential mechanical effects of the porogen leaching and sterilization by EtOH, we conducted preliminary mechanical tests of cylinders soaked in EtOH for 5 days. While specimen integrity was not affected by EtOH exposure, we noted a reduction in the CM and UCS (Figure 3.30). The decrease in CM is 31.8% for pure PCL, 34.3% for 90/10 and 42.5% for 80/20 PCL-CaP composite materials. The decrease in UCS is 60.1% for pure PCL, 58.9% for 90/10 and 56.4% for 80/20 PCL-CaP composite materials. These results suggest that care should be taken to minimize EtOH exposure time during manufacturing.


| (A) | (B) | (C) |
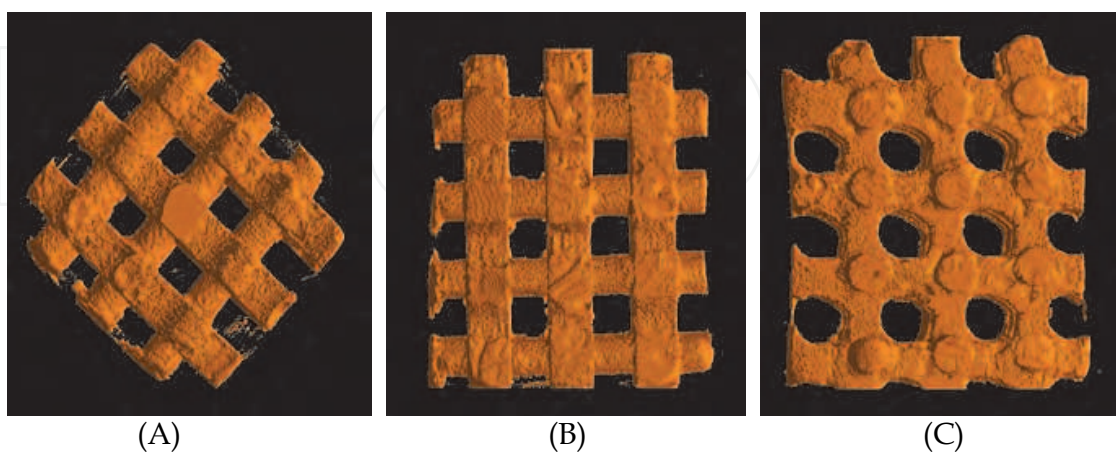
Fig. 9. µCT analysis of 80/20 PCL-CaP composite scaffolds. A: View of horizontal build plane (looking down the longest dimension), note the sharp square pores; B: View of horizontal build plane (looking down shortest dimension), note the sharp square pores; C: View of vertical build plane, note the rounded pores.

(A)   (B)   (C)
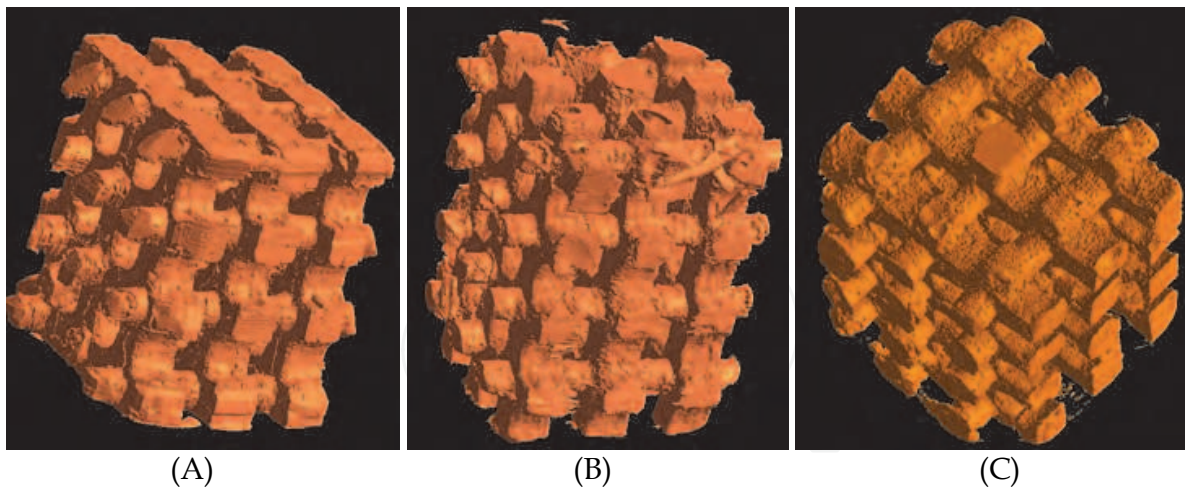
Fig. 10. 3-D reconstruction from µCT data (A) pure PCL scaffold (B) 90/10 scaffold (C) 80/20 scaffold.

ANOVA test for independent variables was used to check for differences between results obtained for different materials. Pure PCL cylinders had average UCS of 12.4MPa and CM of 275MPa. Cylinders with 90% PCL and 10%CaP had average UCS of 19.5MPa and CM of 341MPa, where as cylinders with 80% PCL and 20%CaP had average UCS of 24.8MPa and CM of 425MPa. Increasing stiffness of the material, under compression loading, with the increase of percentage of CaP has been found by the statistical analysis. The UCS increased 57.3% from pure PCL to 90/10 PCL-CaP composite material and 100% from PCL to 80/20 PCL-CaP composite material while the CM increased 24% from pure PCL to 90/10 PCL-CaP composite material and 54.5% from PCL to 80/20 PCL-CaP composite material.
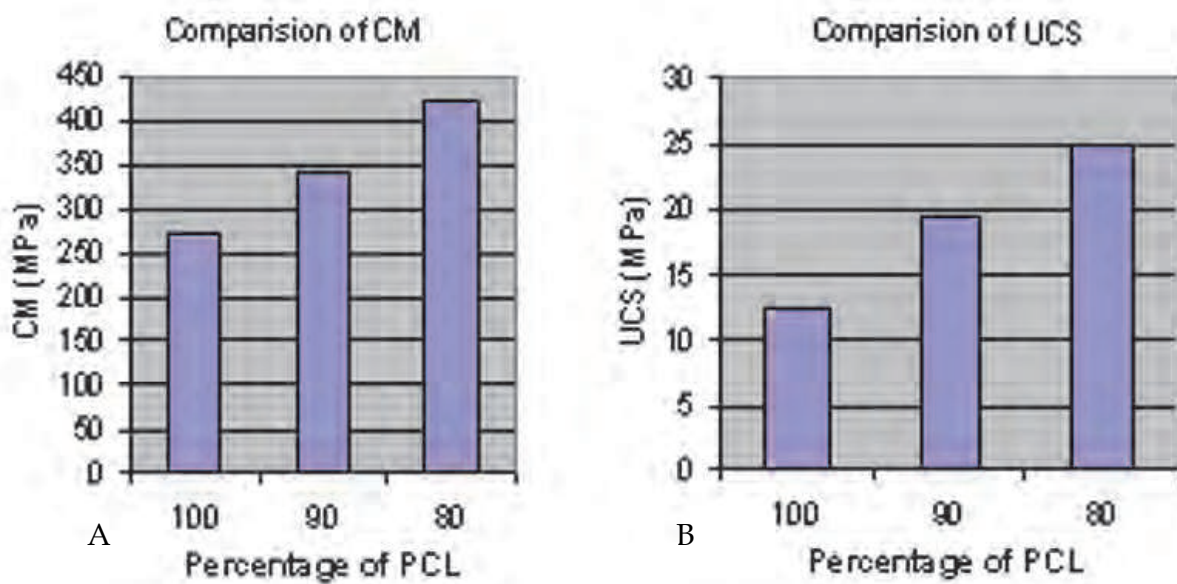
Fig. 11. Compressive mechanical properties of PCL-CaP composite cylinders.
A: Comparison of the compressive modulus of 100% PCL, 90:10 and 80:20 PCL-CaP cylinders; B: Comparison of the ultimate compressive strength with different concentrations of CaP. Statistical analysis indicates that the material properties are significantly different ($p < 0.002$) for different concentrations of CaP.

Comparison of CM for Scaffolds (n=6)

(A)

**Comparison of UCS for Scaffolds (n=6)**
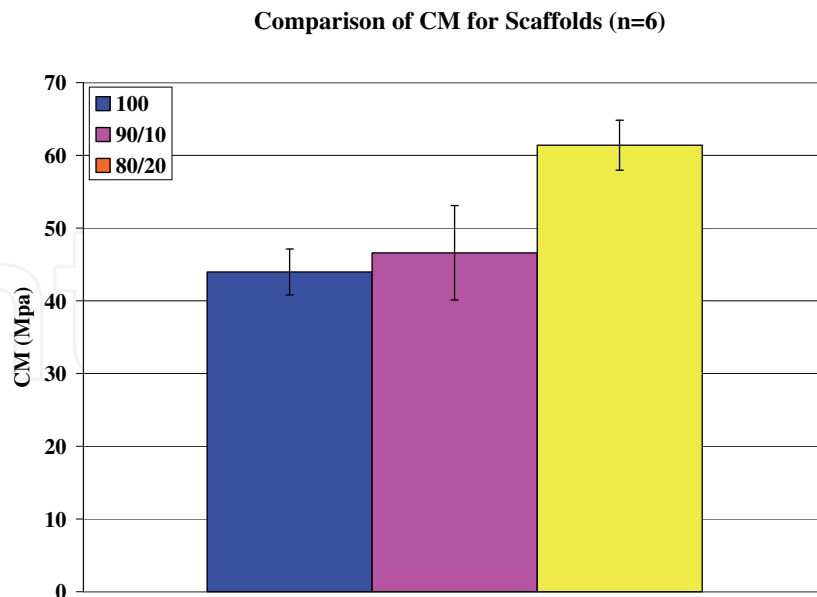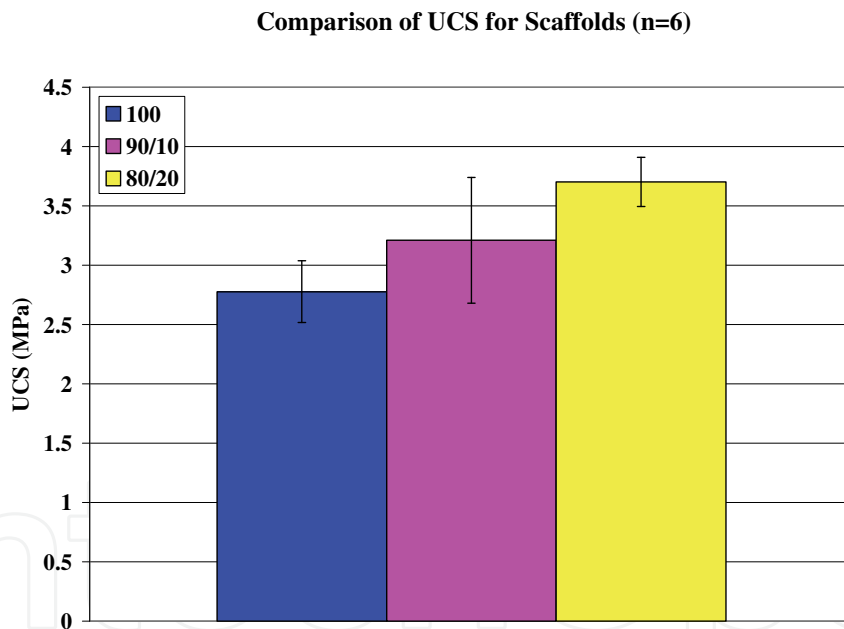
(B)

Fig. 12. Compressive mechanical properties of PCL-CaP composites scaffolds. A: Comparison of the compressive modulus of 100% PCL, 90:10 and 80:20 PCL-CaP scaffolds; B: Comparison of the ultimate compressive strength with different concentrations of CaP.

Figure 12 summarized our compressive testing results for scaffolds with 600μm pores. We noticed the same trend as the cylinders: with the increasing CaP contents, the mechanical performance of scaffolds improved. The 600μm pure PCL scaffolds had UCS values of 2.777±0.26MPa and a CM of 43.97±3.15MPa while the 90/10 PCL-CaP scaffolds had UCS value of 3.21±0.53MPa, CM of 46.6±6.49MPa and 80/20 had UCS of 3.702±0.207MPa, CM of

61.4±3.44MPa Our compressive strength results of the scaffolds with 600μm pores is in line with reported values for trabecular bone from human mandibles ranging from 0.22 to 10.44MPa [Misch, Qu and Bidez, 1999]. We noted that the compressive strength of trabecular bone varies greatly with anatomical location and individual factors such as bone density, volume fraction of the sample being measured, and strain rate [Cater and Hayes, 1976]. Our scaffolds are considerably less stiff than and hence not suitable for replacing cortical bone, for which UCS values of over 200MPa have been reported [Carter and Hayes, 1976]. The small standard deviation (<10% coefficient of variation) for CM and UCS of the solid cylinders as well as scaffolds (except 90/10 scaffolds) demonstrates the reproducibility (in a range of 84-96%) of the mechanical properties achieved using this process. The standard deviation results for compression specimens as well as scaffolds had clearly shown the repeatability of mechanical properties of the products manufactured by the structured porogen method.

The compressive test results can be compared to scaffold mechanical properties reported by others for PCL scaffolds of similar porosity (Table 1). CM was slightly higher than Hutmacher et al. (2001), in the range reported by Zein et al. (2002), and slightly lower than reported by Williams et al. (2005). UCS is essentially equal to 0.2% offset yield stress in our experiments, due to the brittle failure mode of most samples. The mean UCS of our scaffolds was at the high end of the reported range for PCL scaffold yield stress in the literature [Hutmacher et al., 2001; Zein et al., 2002 and Williams et al., 2005]. The CM and mean UCS for 90/10 and 80/20 PCL-CaP composite scaffolds were all higher than reported for PCL scaffolds in the literature [Hutmacher et al., 2001; Zein et al., 2002 and Williams et al., 2005].

	Porosity	Compressive Strength or Yield Stress (MPa)	Compressive Modulus (MPa)
Hutmacher et al. 2001[*]	61.1 %	2.0 – 3.1	21.5 – 41.9
Zein et al. 2002[+]	48 – 77 %	0.4 – 3.6	4 – 77
Williams et al. 2005[+]	63 – 79 %	2.0 – 3.2	52 – 67
Our results	52.5 %	3.15 ± 0.157	45.672 ± 3.798

*:Range of mechanical properties reported reflects differences between two strut lay-down patterns (constant porosity) in either dry condition or wet in saline.
+: Range of mechanical properties reported reflects the dependence on porosity, in both cases the compressive mechanical properties increased with decreasing porosity.

Table 1. Porosity and compressive properties of PCL scaffolds fabricated by various SFF techniques.

2.4.2 Tensile test

Most of bone scaffold testing is based on compression test, because it is the simplest way to evaluate the mechanical properties of bone scaffolds. As we know that the tensile strength is equally important for bone scaffolds. To our knowledge there is no available data for bone scaffolds tensile testing, one reseaon is that the testing aparatus is hard to build and standardized for micro-porous structures. In this study we also tested the tensile strength of the diverse scaffold materials. Followed ASTM standard D638-03 for dogbone tensile bars, with wide ends and a narrow middle, which are commonly used in tensile test, were

designed. The grips of the testing setup hold the specimen tightly at the wide ends. The midsection of the sample has a narrower width than the grip section. This concentrates the stress in the test area, so that fracture and most of the strain occur there. To make the dogbone tensile specimens, a three piece mold was designed. Using this mold, testing specimens were prepared by injection molding, followed by machining operations to assure all surfaces are free of visible flaws and scratches. Numbers of specimens (n≥6) have been tested for each material. Tensile modulus was measured at a tension rate of 5mm/min following the ASTM standard. To find out the literal deformation properties of the various materials, we also conducted Poisson ratio test for PCL, PCL/CaP composite materials. Before the tensile testing, general purpose strain gages (Vishay micro-measurements & SR-4) were mounted on each specimen to measure the Poisson's ratio. Since the strain gauge is an extremely sensitive device and any small imperfection in the bond can affect the performance, extra caution was taken when installing the gauge onto specimens. During the tests, the specimens that broke due to flaw, or that broke outside of the narrow cross-sectional test section were discarded. The width and thickness of the flat specimens at the center of each specimen have been measured and recorded before test. Then the specimens have been placed in the grips of the testing machine. The grips have been tightened evenly and firmly to prevent slippage of the specimen during the tests. Tensile strength and tensile modulus were computed as the slope of the stress-strain curve. Figure 13 shows a typical tensile stress-strain curve for 90/10 PCL-CaP dogbone specimen. As seen in Figure 14 the increase in CaP concentration of the composite significantly raised the tensile modulus (TM) and UTS as well as stiffness of the material of the samples ($P<0.002$). There was an approximately 8% of increase in UTS from pure PCL to 90/10 PCL-CaP composite material and 52.6% increase in UTS from pure PCL to 80/20 PCL-CaP composite while the TM increased 11.4% from pure PCL to 90/10 PCL-CaP composite material and 22.9% from pure PCL to 80/20 PCL-CaP composite material.

ANOVA test for independent variables was used to check for differences between results obtained for different materials. Pure PCL dogbones had average UTS of 1.90±0.19MPa and TM of 105±15.4MPa. Dogbones with 90% PCL and 10%CaP had average UTS of 2.05±0.35MPa and TM of 117±17.8MPa, where as dogbones with 80% PCL and 20%CaP had average UTS of 2.90±0.31MPa and TM of 129±17.8MPa. It has been found statistically that by increasing percentage of CaP the tensile strength of the material increased.

Poisson's ratio was calculated using the recorded transverse contraction strain to longitudinal extension strain. The results were summarized in Figure 15. The Poisson's ratio behavior of the various materials under tension showed a general trend of decrease with increasing CaP content. The testing results were within the range for silicone and some polymers such as acrylic and polycarbonate.

In addition to testing the tensile properties of dogbone specimens made of the diverse scaffold materials, we also tested the tensile strength of pure PCL scaffolds with 600μm pore size using the same testing machine. The reason we only performed one material tensile testing for scaffolds is that the standard tensile testing procedure is very hard to follow, the scaffold fixtures are very difficult to fulfill and the time limitation. Three specimens were used for testing and they were pulled to failure. Figure 16 showes a typical tensile stress–strain curve for PCL scaffold. In order to test tensile properties of the scaffolds, a fixture with two ends has been designed (Figure 17) which has a narrow bar end for the gripper to
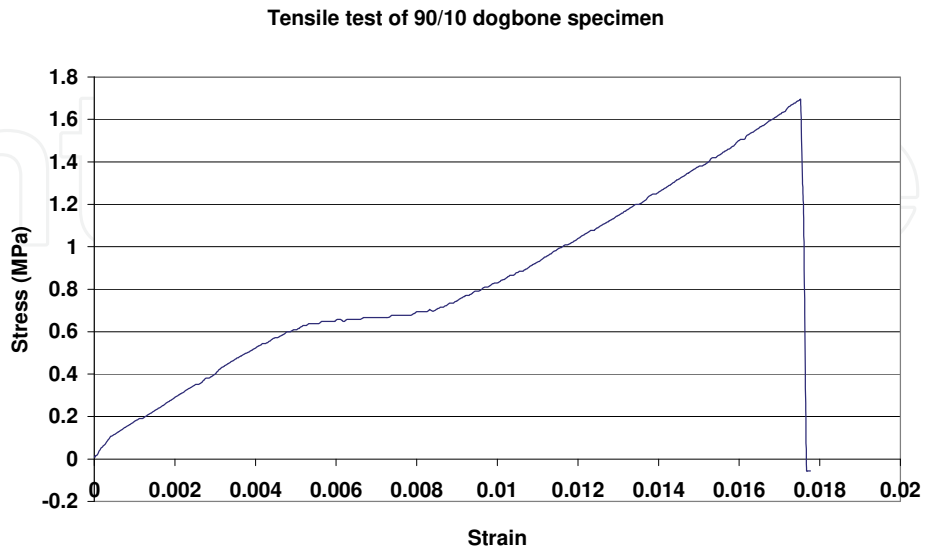
Fig. 13. Tensile stress-strain curve for a 90/10 PCL-CaP dogbone specimen.
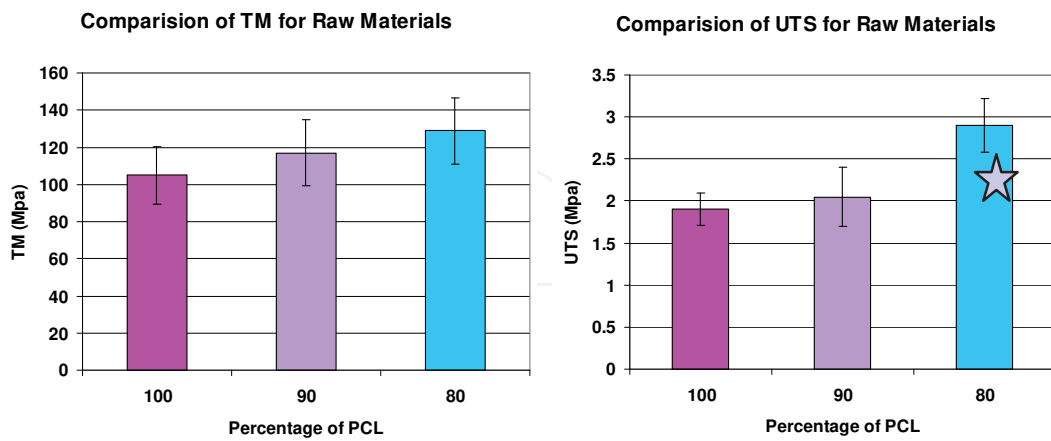
Fig. 14. Tensile mechanical properties of PCL-CaP composites (n≥6). A: Comparison of the tensile modulus of 100% PCL, 90:10 and 80:20 PCL-CaP scaffolds; B: Comparison of the ultimate tensile strength with different concentrations of CaP.

Poisson's ratio measurement

(A)

Stress-strain curve of tensile test for scaffold

(B)
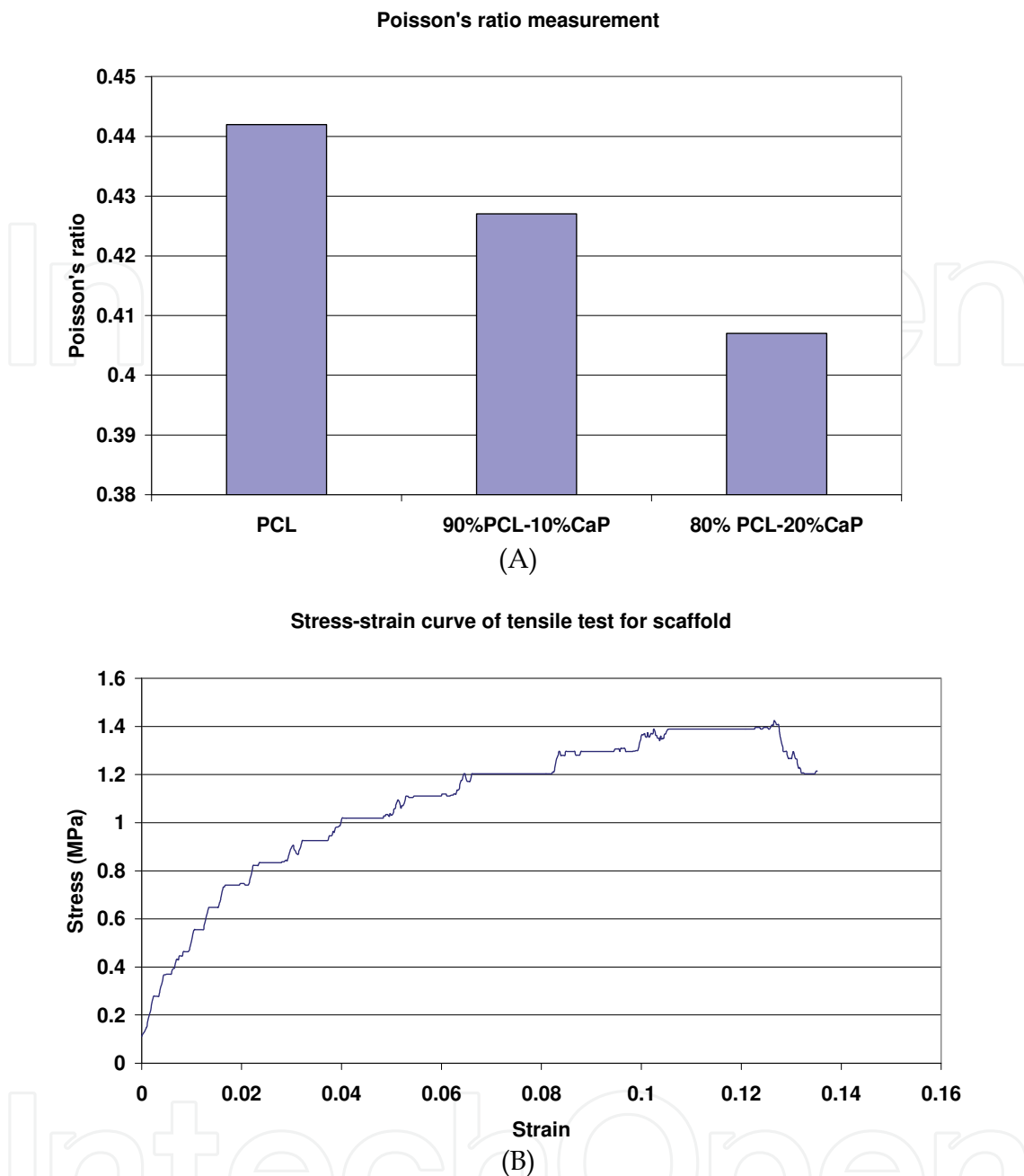
Fig. 15. Poisson's ratio measurement results. Figure 16: Tensile stress-strain curve for a PCL scaffold with 600μm pores.

easily grip. Epoxy was used to glue the scaffolds onto the fixture one day prior to the test. The epoxy has to have enough strength to withhold the load and the viscosity can not be too low so it won't block the pores. At the same time the strength and capillary effect of the epoxy has been tested before tensile tests. An acceptable epoxy was selected (Epoxy adhesive 300, Rosco laboratories Inc). Porous scaffolds with a dimension of ~ $6.6 \times 6.6 \times 13.8$mm^3 were used (Figure 18A). A porogen (Figure 18B) has been designed to make the longer scaffolds for tensile tests using the aforementioned injection method. The 600μm pure PCL scaffolds had UTS values of 1.43 ± 0.35MPa and a TM of 25.70 ± 0.47MPa. We noted that the tensile properties of the materials and scaffolds are significantly lower than the compressive properties.

(A) (B)
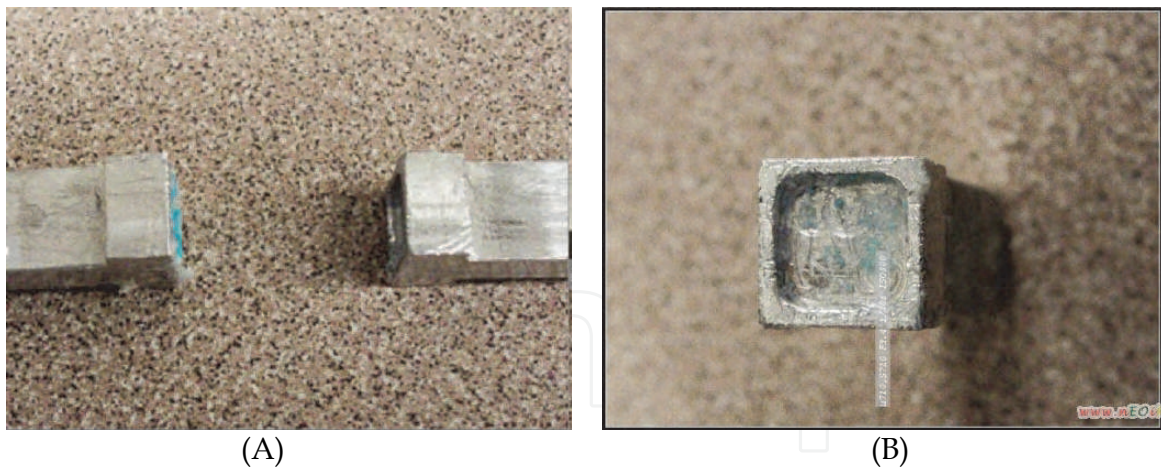
Fig. 17. Designed fixture for tensile testing: (A) Two ends of the scaffold holder (B) Top view of single scaffold holder to show the cavity for mounting the scaffold.


(A) (B)
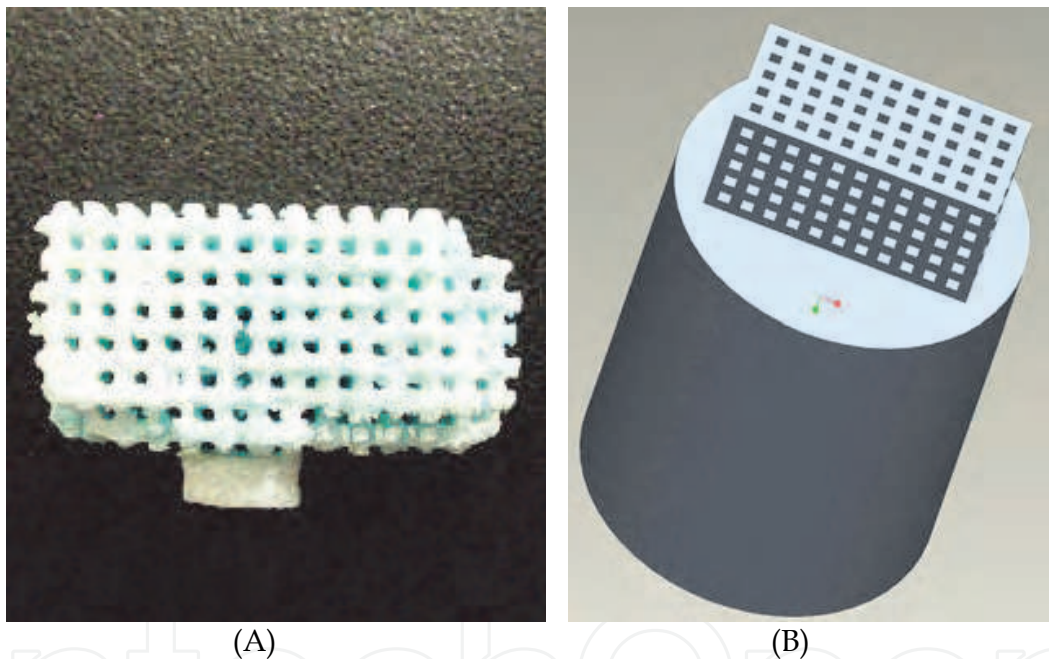
Fig. 18. (A) PCL scaffold for tensile testing (B) CAD design of porogen to make long scaffold for testing.

2.5 Biocompatibility test

To test the cytocompatibility of the scaffolds made by our structured porogen method using DDP system human embryonic palatal mesenchymal (HEPM) cells (ATCC, CRL-1486) were used in this part of study.

2.5.1 Testing protocols

HEPM cells are routinely maintained in Eagles' minimum essential medium (MEM) with Earles' salts supplemented with 10% fetal bovine serum (Hyclone), 2.0mM L-glutamine, 1.0mM sodium pyruvate, 0.1 mM non-essential amino acids, and 1.5 g/L sodium bicarbonate at 37°C in a 5% CO_2 incubator [Li et al. 2005]. For cell culture studies, the

fabricated scaffolds were sterilized with 70% ethanol for 1 hour at room temperature, and washed 3 times with sterile phosphate buffered saline (PBS). The scaffolds were then incubated with a mixture of 30µg/ml collagen type I (BD Biosciences) and Matrigel™ (BD Biosciences, diluted 1:30) in MEM for 1 hour at 37°C to facilitate ECM protein adsorption and enhanced cellular attachment. Scaffolds were then seeded with a suspension of 1 million HEPM cells/ml overnight on an orbital shaker (Belly Dancer, Stovall). Following seeding, scaffolds were transferred to 24-well plates, allowed to equilibrate for 2 hours in the described cell culture medium and the initial level of cell seeding was assessed by the Alamar Blue™ (Biosource) assay [Li et al. 2005] which incorporates a fluorometric/colourimetric growth indicator that both fluoresces and changes color in response to chemical reduction of growth medium resulting from cell growth based on detection of metabolic activity. In order to evaluate cell proliferation on the various scaffolds the Alamar Blue™ assay was performed again on the same samples at day 4 post-seeding. Subsequently, the samples were fixed in 10% buffered formalin (Fisher Scientific) for 1 hour at room temperature and stored in PBS at 4°C until cytological staining. For staining, the samples were washed once more with PBS and incubated with PBS containing 2µg/mL Hoechst 33258 (Bisbenzimide, Sigma), a nuclear stain.

2.5.2 Results and findings of biocompatability testing for PCL and PCL-CaP scaffolds

HEPM cells growing on the scaffolds are visualized by fluorescent staining of cell nuclei, and SEM. In the case of 3-D scaffolds of PCL and 80/20 PCL–CaP, HEPM cells were able to attach as evidenced by fluorescent nuclear staining with Hoechst 33258 (Figure 19). These images indicate attachment onto the struts of both PCL (Figure 19A) and 80/20 PCL–CaP composite scaffolds (Figure 19B). Based on the Alamar Blue™ data, the initial seeding efficacy was not significantly different for the materials used (data not shown). This similar level of HEPM cell attachment to all materials used was probably due to the fact that all scaffolds were pre-coated with a mixture of Matrigel™, a reconstituted extracellular matrix, and collagen type I solution. Without this coating, cellular attachment to the synthetic surfaces was minimal only (data not shown). Once attached, HEPM cells proliferated on all types of 3D scaffolds, as assessed from the Alamar Blue™ (AB) fluorescence data (Figure 20), with some differences between materials. The normalized cell proliferation data indicated an identical cell proliferation on pure PCL and 90/10 PCL–CaP scaffolds. By contrast, cell growth on the 80/20 scaffolds was significantly enhanced ($p<0.05$). The AB data was validated qualitatively by the observed increase in the density of Hoechst 33258–stained nuclei following 4 days of post-seeding culture in *vitro* on the various scaffolds (Figure 21). We note that at this time point, cells were visibly growing both on the struts (Figure 21A and C), as well as in the interior pore structures of all scaffolds investigated (Figure 21B and D). For further confirmation of cellular ingrowth into the scaffold center, the scaffolds were cut into segments using a scalpel. The presence of cells on all interior surfaces was visualized by nuclear staining (Figure 21E).

The morphology of HEPM cells growing on PCL and 80/20 PCL–CaP composite scaffolds was assessed by SEM. As seen in Figure 22A the cells flattened on the rather smooth PCL surface. By contrast, on the 80/20 PCL–CaP the cells seemed to form multilayer assemblies (Fig. 22B), which further corroborates the increased density of nuclear staining (Figures 20 and 21) and significantly higher level of cell proliferation (Figure 21) as compared to 100% PCL. In summary, these cytocompatibility tests clearly indicate that all structured porogen scaffolds when coated with suitable ECM proteins facilitate attachment and support proliferation of HEPM cells *in vitro*. In addition, our data suggest that the presence of CaP in

the PCL–CaP composite enhances the proliferation of HEPM cells and reduces their spreading in favor of multi-layer assembly.


(A)   (B)
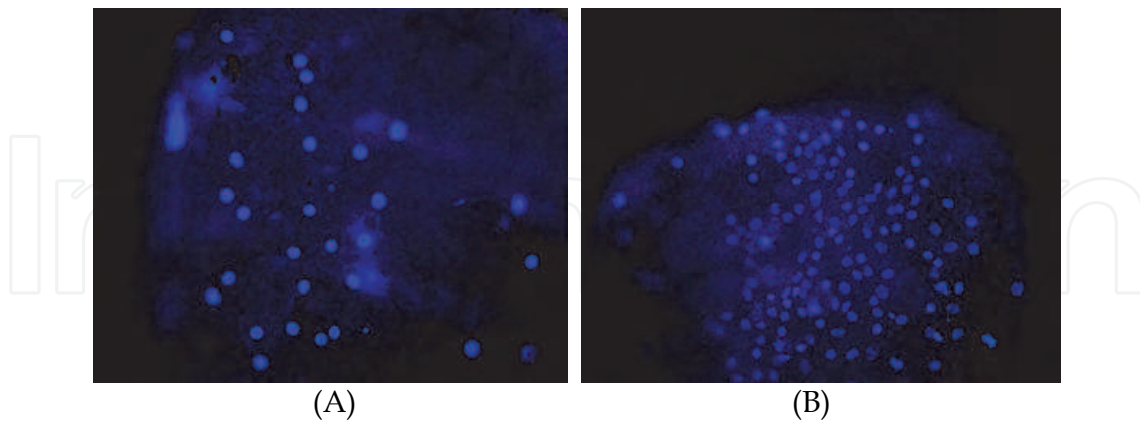
Fig. 19. Bisbenzimide nuclear staining of adherent HEPM cells following 24 hours of orbital shaker seeding on PCL (Panel A, 200x) and 80/20 PCL-CaP composite (Panel B, 100x) scaffolds, 600 μm pore sizes. Images are captured by imaging the surface of a strut on the outside of the scaffold.


Fig. 20. Normalized increase in Alamar Blue™ readings over the 4 day *in vitro* culture period following the initial 24 hour seeding period for 600 μm pore size pure PCL, 90/10 and 80/20 PCL-CaP scaffolds. Metabolic activity as measured by Alamar Blue™ at 96 hours post-seeding was normalized to the Alamar Blue™ readings taken immediately following the 24 hour seeding period. Y-error bars represent the standard deviation from the mean for each sample (n = 5). * = Statistically significant differences ($P < 0.05$) compared to 100% PCL by one-way ANOVA with Tukey-Cramer post-tests for multiple comparisons.

(A)

(B)

(C)

(D)

(E)
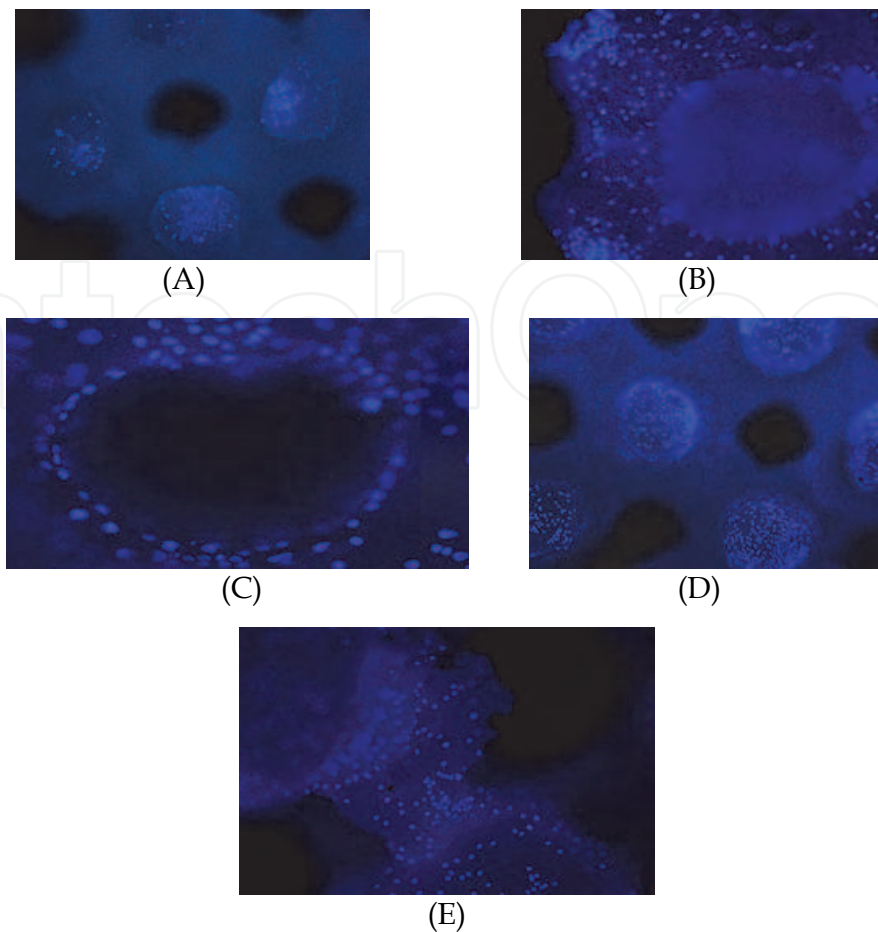
Fig. 21. Bisbenzimide staining of HEPM cells cultured on PCL (Panels A and B) and 80:20 PCL-CaP composite (Panels C and D) scaffolds for 5 days. A: HEPM cells on the surface struts of a 600 µm pore size PCL scaffold (50x); B: HEPM cells growing around and into a pore on the same scaffold imaged in panel A (100x); C: HEPM cells on the surface struts of a 600 µm pore size 80:20 PCL-CaP composite scaffold (200x), note the increased density of nuclear staining relative to the PCL scaffold; D: HEPM cells colonizing a pore in the scaffold imaged in panel C (original magnification 50x); E: HEPM cells growing on a strut from the scaffold center (100x).

(A)

(B)
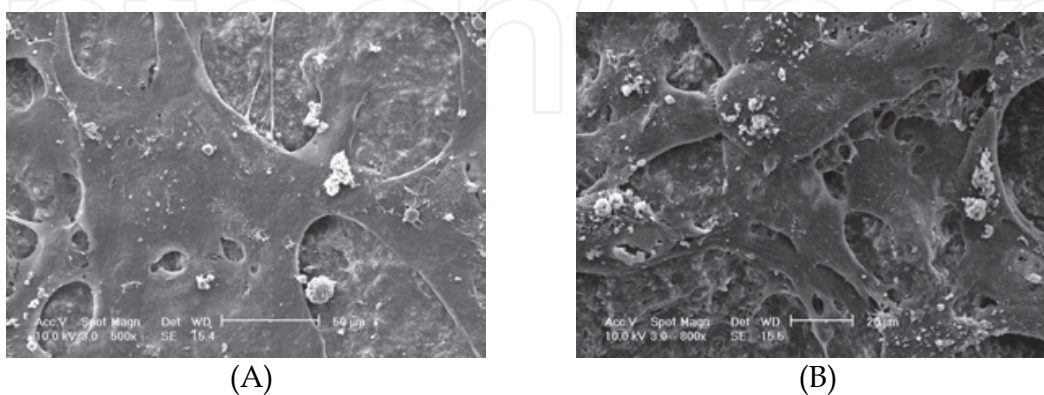
Fig. 22. Scanning electron micrographs of HEPM cells cultured on 600 µm pore size PCL and 80/20 PCL-CaP scaffolds for 5 days. A: Flattened HEPM cells on PCL scaffold, Scale bar = 50 µm; B: Multilayered HEPM cells on 80/20 PCL-CaP scaffold, scale bar = 20 µm.

Biocompatibility has been demonstrated for PCL, PCL-CaP scaffolds fabricated using the structured porogen method by DDP. Our findings are in line with previous reports showing that PCL scaffolds fabricated using various manufacturing processes display good cytocompatibility *in vitro* [Darling and Sun, 2004 and Hutmacher et al., 2001] and are biocompatible *in vivo* [Williams et al., 2005]. For example, Williams et al. (2005) used SLS to fabricate PCL scaffolds which were then seeded with human gingival fibroblasts genetically modified to express bone morphogenetic protein-7 (BMP-7) and implanted into subcutaneous pockets of immunocompromised mice. These scaffolds supported the development of new bone over a 4-week period, as evidenced by μCT detection of mineralized tissue [Williams et al., 2005]. Darling and Sun (2004) reported that precision extrusion-deposited PCL scaffolds supported the proliferation of cultured rat cardiomyoblasts, however detailed analysis of cellular metabolism, proliferation, and morphology were not provided. Hutmacher et al. (2001) used primary human fibroblasts and human osteoprogenitor cells to demonstrate the biocompatibility of PCL scaffolds fabricated by fused deposition modeling, although the capacity of these scaffolds to induce bone formation was not addressed.

Diverse scaffolds fabricated from CaP and diverse CaP composites also display *in vitro* [Wang, Tian, Liu, Cheng, Liao and Lin, 2005 and Xu and Simon, 2005] and *in vivo* [Ruhe, Hedberg, pardon, Spauwen, Jansen, Mikos, 2005] biocompatibility. For example, Wang et al. [Wang et al., 2005] demonstrated that biomimetic nano-structured CaP scaffolds, fabricated by gel lamination technology, supported osteogenic differentiation, as evidenced by alkaline phosphatase expression. Xu et al. (2005) used a murine osteoblast cell line to demonstrate biocompatibility of CaP–chitosan composites with amorphous architecture and pore sizes of 165–270 μm. These scaffolds were fabricated by preparing a water-soluble mannitol—CaP–chitosan mixture and subsequent removal of mannitol to create the pore structure. Amorphous poly (lactic-co-glycolic acid) PLGA– CaP scaffolds of various weight ratios, fabricated by admixing PLGA microparticles into Ca-P cement and implanted into subcutaneous and cranial defects in rats, facilitated fibrovascular and bone tissue development over a 12-week period, respectively [Ruhe et al., 2005]. Compared to these amorphous CaP scaffolds, the primary advantage of our fabricated scaffolds by structured porogen method is that they are comprised of precisely generated structures which allow for reproducible scaffold fabrication and control of mechanical properties.

3. Porogen-based method study using three dimensional printing

The melting point of wax building material of previously used in DDP system is low (75°C), so the biomaterials can be melted and cast into the desingned porogens are limited and the used machine's production speed is relatively low (it takes approximately 15 hours to build a 20x20x20 mm³ porogen). In order to extend the proposed structured porogen method to other commercially available SFF machines and to test if this method can be a universal method on different SFF machines, three dimensional printing (3DP) system was used to test our porogen method in this study. The main reason is that the RP machine uses plaster composite material as building material which has very high melting temperature (in the range of 1400-1500°C) and the building speed of this 3DP system is relatively high ((it takes approximately 1 hour to build a 20x20x20 mm³ porogen).

3.1 Introduction of three dimensional printing (3-DP)

3DP was developed at MIT (Massachusetts Institute of Technology), and it is often used as a direct manufacturing process as well as for rapid prototyping. 3DP creates 3-D object by inkjet printing liquid adhesive to join loose powder, which allows parts to be built very quickly and inexpensively. This technology uses ink-jet based process. The multichannel print head deposits liquid adhesive binder onto the top of a bed of powder object material. The powder is bonded together in the areas where the adhesive is printed. The material used in this application is calcium sulfate hemihydrate plaster based composite powder (ZP 130) and water-based binder (ZB 58). The designed 3-D porogen model was first converted to a general STL format and input into the 3D printing control software for fabrication.
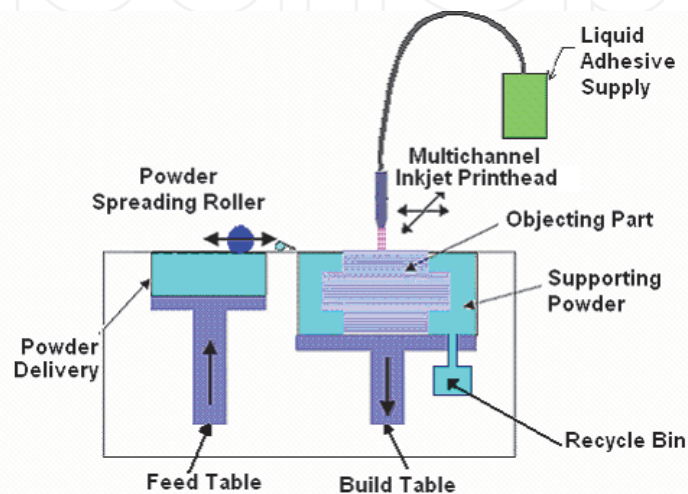
Fig. 23. Schematic overview of three dimensional printer.

A 3-D printer is shown schematically in Figure 23. The system consists of the following units: feed table, build table, spreading apparatus (roller) and multi-channel print head. The feed table is used to measure and dispense powder that is spread across the build table by means of a roller. The building process starts by spreading a layer of powder object material at the top of a fabrication chamber. Once the initial layer is spread, the lowest cross section of the part is subsequently printed by depositing a liquid adhesive binder solution on the powder substrate which becomes bonded in the areas where the adhesive is deposited, to form a layer of the object by means of a multi-channel jetting head on the print head gantry in a 2-D pattern. Once a layer is completed the build table moves down and the feed table moves up one layer thickness to supply powder for the process. The roller then spreads and compresses the powder at the top of the building chamber. The process is repeated until the whole object is completed. Once the part has been completed and the part has been allowed to dry sufficiently, then the part can be removed and excess powder can be brushed off of the part. No support material is needed because the surrounding powder in the build chamber acts as support structure during fabrication. Once the part is de-powdered, infiltration can be used to increase part strength and achieve a desirable finish.

3.2 Porogen design and fabrication
3.2.1 Porogen design

Porogen with small voids were designed using Pro/E CAD design software and constructed to evaluate the machine resolution of 3-DP porogen approach. This inkjet 3-D printing

technique allows the designing and fabrication of porogens of various patterns, pore sizes, and porosity. In this part of the study, rectangular and round shaped honeycomb-like porogens were fabricated. Figure 24 shows the design architectures of the porogens. The strut size ranges from 200 to 400 μm. To examine the machine resolution in the porogen 3-DP approach, first a porogen with 200μm struts spaced 800μm apart was designed, Fig. 24A. After fabrication, we noticed that the 200μm struts can not be formed (it's too thin). Then we increased the strut size to 300μm (Fig. 24C), and we observed that the porogen can be manufactured, but struts were too weak to hold any force. With further increasing the strut size to 400μm, good porogens with acceptable struts quality were produced. A taller porogen was designed at the beginning (Fig. 24E), but the excess powder was very hard to clean out completely. At the end a final porogen with 400μm struts, 800μm voids and overall dimension of 10.4×10.4×6.2 mm was designed (see Fig. 24F).

3.2.2 Porogen fabrication

Once the design was completed, the STL file was imported into the 3-D printer and sliced into layers. A commercially available 3-D printer (Z310 plus, Zcorp) was used to print each layer sequentially. The Z-Printer functions by selectively gluing layers of powder together. During fabrication, the liquid adhesive was selectively printed on an 89μm thick layer of plaster powder to form the 2-D pattern. This process was repeated until the porogen was completely printed. Following the printing stage, the individual porogens were removed and then cleared of excess powder which filled into the pores, using pressurized air blower, and then prepared for injection. To help the biomaterial injection, a hollow cylindrical injection tool with 400 μm opening on the top and a basin with 10.4 mm internal diameter was designed and fabricated separately which allows the plunger of a standard plastic 1ml syringed could be used to inject the molten biomaterials into the pores of the porogen. The porogens and the injection tool were sintered at 275°F for 30 minutes. Following sintering, the porogens were infiltrated with alginate or polyethylene glycol (PEG, Sigma) to strengthen the porogens and to fill the small surface pores. 3% (W/V) alginate was prepared prior to infiltration by using alginate acid salt (Sigma) and 1% acetic acid. 20% and 40% (W/V) PEG were also prepared by using PEG pellet and DI water. The reason to choose alginate and PEG as infiltration materials is because they all are biocompatible and PEG is water soluble biomaterial. The solvent we used to remove the plaster can remove plaster and alginate, so there will be no any infiltration residul left on the fabricated scaffold. All solutions were made and stirred for 60 minutes at room temperature. The porogens were dipped into the solutions for 2 seconds and quickly removed from the solutions. The infiltrated porogens were air dried at room temperature and collected into a capped tube. Then the coated porogens were prepared. Half of the pores of the alginate infiltrated porogens were clogged by alginate. The alginate did not penetrate to the plaster porogens, so alginate is not a good choice for infiltration. The resultant 20% PEG infiltrated porogens were much better, the capillary effect helped the PEG solution to fill the micropores on the wall, but still left the macropores open. The only problem with 20% PEG was the water contents were too high, so it was very easy to destroy the porous structure. The 40% PEG infiltrated porogens were the best, not only because the small microspores on the surface were all filled, but also because the structural integrity of the whole porogen was kept. In the late study, all the porogens made of 3-DP were infiltrated by 40% PEG. The printed and infiltrated porogen are shown in Figure 25.
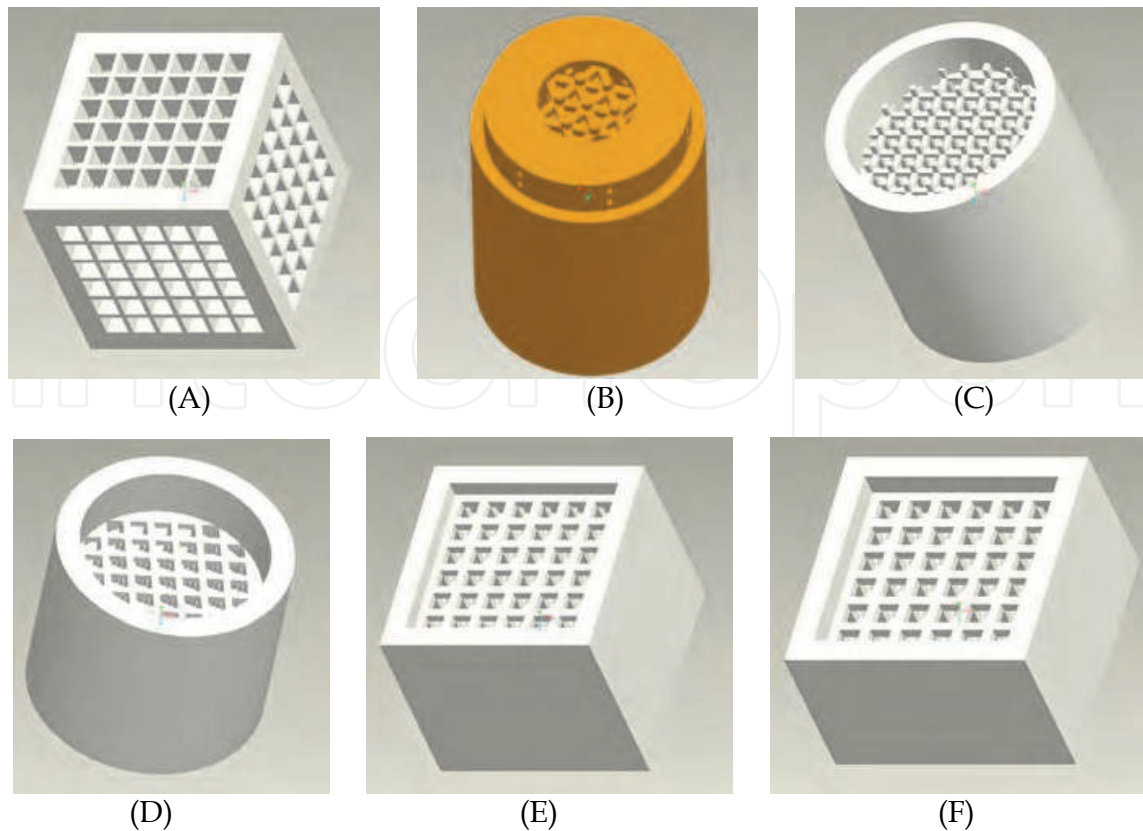
Fig. 24. The designed porogens: (A) Square porogen with 200μm struts spaced 800μm apart (B) 0/60°/120° lay down pattern (C) Round porogen with 300μm struts spaced 800μm apart (D) Round porogen with 400 μm struts spaced 800μm apart (E) Square tall porogen with 400μm struts spaced 800μm apart (F) Square short porogen with 400μm struts, 800μm voids and overall dimension of 10.4×10.4×6.2 mm.
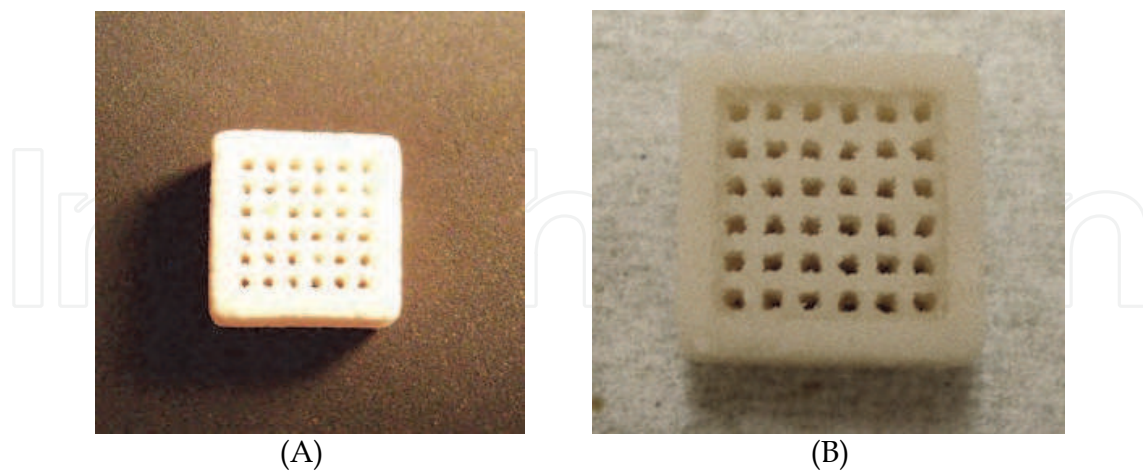

Fig. 25. Pictures of (A) Printed plaster porogen (B) PEG infiltrated porogen.

3.3 Fabrication of bone scaffolds
3.3.1 Scaffold fabrication
PCL pellets were weighed using a standard balance, as well as a calculated amount of CaP powder based upon how much PCL was measured and the desired ratio of the composition.

Then the two weighed materials were mixed in a glass beaker. Pure PCL, 90/10 and 80/20 PCL–CaP were melted at 75°C in the oven, respectively. The melted composites were stirred for half an hour by using an ultrasonic probe to ensure the composition was mixed evenly and any small sample from the beaker would be made up of the desired percentage. Half an hour before scheduled injection, the mixtures were subjected to a vacuum in order to minimize air bubbles in our scaffolds. After that the melted material was injected into the infiltrated porogens using disposable 1ml syringe by pressing the injection tool tightly onto the porogen. The injected porogens were cooled at room temperature. The excess solidified material was cleaned using a razor blade. Cavex GreenClean Alginate and Plaster Remover solution was prepared by measuring two scoops of biodegradable Cavex powder in 500ml lukewarm water. Porogen material was removed by submerging the injected porogens in the mixed solution. Each injected porogen was immersed in 50ml filled tube and placed in a rotator with a setting temperature of 40°C. The solution was changed every 24 hours. After 5 days of immersion, the scaffolds were taken out from the tubes and air dried. The resultant scaffolds then were washed in DI water for 20 min. Then the scaffolds were collected for future tests. Figures 26 shows the SEM images of porogen, infiltrated porogen and resultant scaffolds. The pores on the scaffolds were observed. The pores on infiltrated porogen are more regular shape comparing with the porogen without any treatment. The infiltration not only helped to improve the mechanical strength of the porogen, but also helped to improve the quality of the resultant scaffolds.

3.3.2 Femur head fabrication

To further explore the compatibility of making complicated scaffolds using the structured porogen method by 3-DP, a femur head was fabricated by casting PCL into the plaster mold. A CAD model has a negative shape of reconstructed femur head. Figure 27A shows a picture of the plaster femur head mold and Figure 27B&C show two views of the fabricated PCL femur head by 3-DP.


| (A) | (B) | (C) |
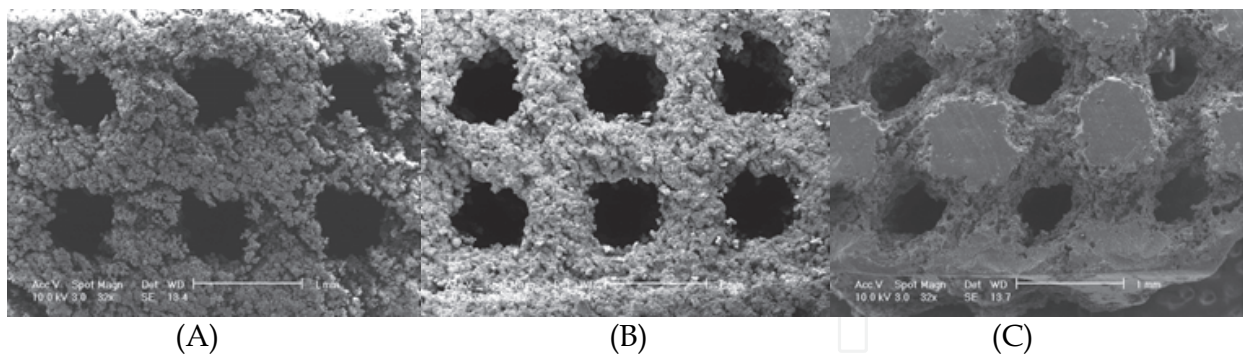
Fig. 26. SEM images of (A) Porogen (B) Infiltrated porogen (C) PCL-CaP composite scaffold from 3-D structured plaster porogen.

3.4 Toxicity test

During the porogen material removal process the reaction of Cavex plaster remover and plaster might bring some unknown reactant into the scaffolds, therefore a toxicity test was perfomed in this part of study. Following standard protocols, cell viability has been continuously quantified by Alamar Blue™ assay. 7F2 and EAhy 926 have also been cultured in standard medium without extract as controls. Cells have been cultured in 24 well plate for
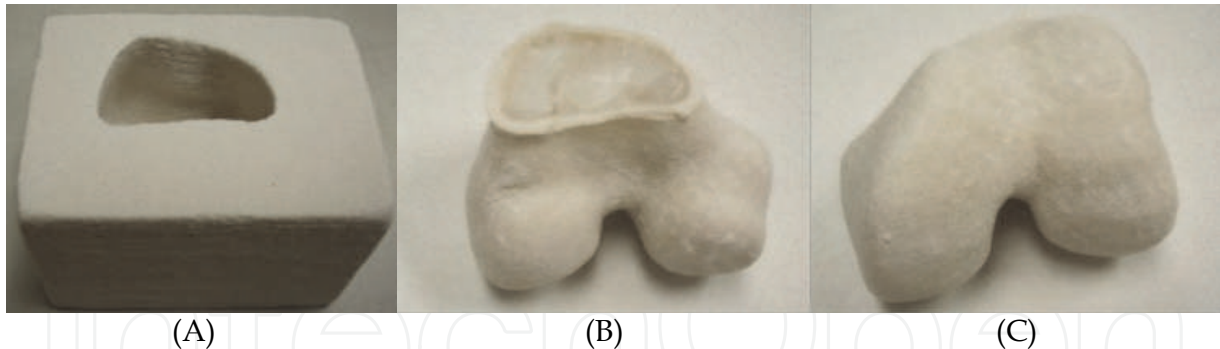
Fig. 27. A: 3-D printed plaster femur head mold; B&C: Front and bottom view of Injected PCL femur head.

4 days (n=3 wells for each cell in each kind of medium). The Alamar Blue™ assay was performed every two days. The result shown in Figure 28 indicates that the 7F2 and EAhy 926 cells did not experience any significant cellular dysfunction due to the degradation product of PCL scaffolds. ANOVA test for independent variables was used to check for differences between results obtained for different mediums which showed no significant change between the controls with the testing mediums.

4. Structured porogen method by a newly developed sucrose printing RP machine

The commercially available SFF systems we used previously are all using non-biocompatible materials such as thermal plastic wax (Solidscpe Inc.), plaster (Z-corp), photoresin (3D system Inc.) etc., and the porogen dissolving process is complicated and time consuming. Most importantly, porogen materials cannot be completely cleaned up; and their residues will stay with final scaffolds and will have negative effects on scaffold's bioactivities. To overcome the above mentioned problems we have designed and developed a novel biomaterial-sucrose deposition system and used this system to fabricate structured porogen.
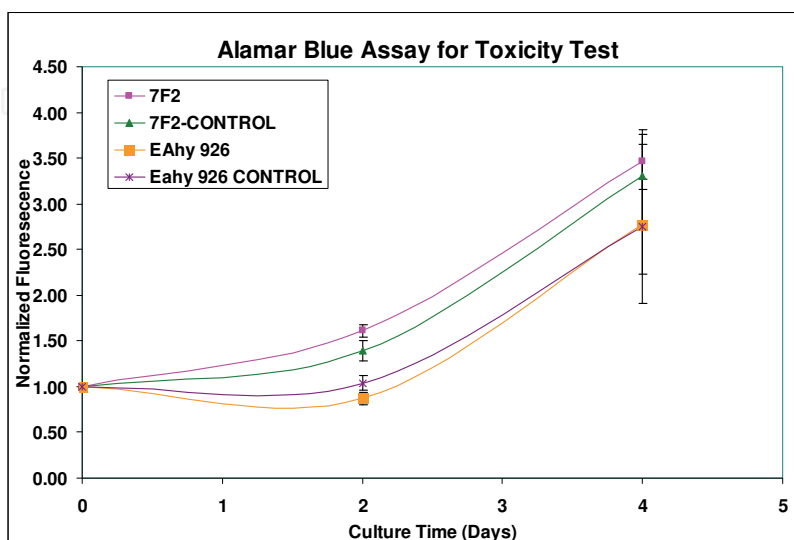

Fig. 28. Toxicity testing result for PCL scaffolds.

4.1 Porogen material study-sucrose mixture and the functions

The most important task of this part of study was to develop a versatile SFF based fabrication system that can deposit biocompatible and easy-washing clean material for porogen fabrication. Sucrose is one of the most abundant carbohydrates found in nature and is a major component of the food chain [Sturgeon, 2003]. Sucrose has the empirical formula $C_{12}H_{22}O_{11}$ and a molecular weight of 342.30. Sucrose is easy to clean, because it is highly soluble in water, and is also somewhat soluble in alcohol and other polar solvents. The saturated solutions of sucrose in water and ethanol at 20°C are 67.09 and 0.90 percent by weight, respectively. However, it is generally insoluble in non-polar solvents. It is slightly soluble in methanol and insoluble in ether dioxine and chloroform. This selective solubility in different solvents provides a convenient processing manipulation, and will enable a polymer composite solution to be injected into the porous sucrose structure without destroying its structural integrity. The sucrose progen/skeleton can be removed by using water leaching after the composite being solidified. At room temperature, sucrose is a monoclinic crystal and it melts at 185°C, and decomposes when heated above 200 °C [Yudkin, Edelman and Hough, 1971]. Due to its natural biocompatibility, sucrose has found broad applications in tissue engineering [Ma, Wang, He and Chen, 2001 and Li, Tuli, Okafor, Derfoul, Danielson, Hall and Tuan 2005].

In this study, we selected our modified sucrose as a porogen material in terms of its bioresorbability, fluidity, and manufacturability. For this, we first melt the porogen material until it reached a semi-liquid state and then extruded it through a nozzle on the substrate or underlying layer to form one layer of the part. To extrude the porogen material, a sucrose mixture was developed, which consists of sucrose, honey, alum and butter. This mixture has met the requirements for our porogen material. Alum (Aluminum Sulfate $Al_2 (SO_4)_3$) can reduce the melting temperature of the mixture. Honey can also reduce the melting temperature and increase the hardness and the viscosity of the mixture. Butter was also added to work as lubricant.

4.1.2 Sucrose solution preparation process

Water and sucrose were heated together to 100°C until almost no water was left, and then honey and butter were added. The mixture was reheated to 85°C, and then alum was added. In this study, it has been found that the melting temperature of the modified sucrose mixture reduces to around 80°C, where the material has low viscosity and good fluidity, and is easily extruded from the nozzle to form fine fibers. The deposited sucrose fibers solidify at room temperature. The viscosity of our porogen material was measured for shear rates changed from 220 to 2200 s-1. Table 2 shows that with changing the ratio of each component of sucrose mixture, we could get different viscosity result. The water contents had the biggest effect on the viscosity results. With the ratio of sucrose, honey, alum, and butter setting to 90:4:5:1 by weight, we performed the rheology test.

Mixing	Sucrose (g)	Alum (g)	Honey (g)	Butter (g)	Water (g)	Viscosity (cP)
1	25	1.25	1	0.25	5	5100
2	25	1.25	0	0.25	10	2200
3	25	2	0	0.25	50	270
4	25	0.25	0	0.25	75	40

Table 2. Viscosity of various sucrose mixtures.

4.2 SFF system design

The new SFF system design started with the nozzle jet selection and installation, which includes the nozzle, the heating element of the nozzle and reservoir. We have studied and developed a SFF-based manufacturing system to build our sucrose skeleton which serves as the bone scaffold porogen, and then to extrude and cast the polymer-ceramic composite into the sucrose porogen to form bone scaffolds with predefined structures and sufficient mechanical strength. The schematic of the SFF-based porogen fabrication system is shown in Figure 29. The control signal is sent from the host computer to move the nozzle in *x-y* directions based on the tool path, which was mounted on the moving stage. Air supply was connected with two regulators to provide compressed air for both the porogen material despensing and the valve control. The porogen material reservoir was wrapped in a band heater (Omega Engineering INC, Stamford, CT) which was controlled by a temperature controller (Omega). A custom-made copper needle tip was installed on the microvalve which can be heated up to the same temperature as the microvalve. The heated porogen material was then dispensed on the working stage which can move in *z*-direction.
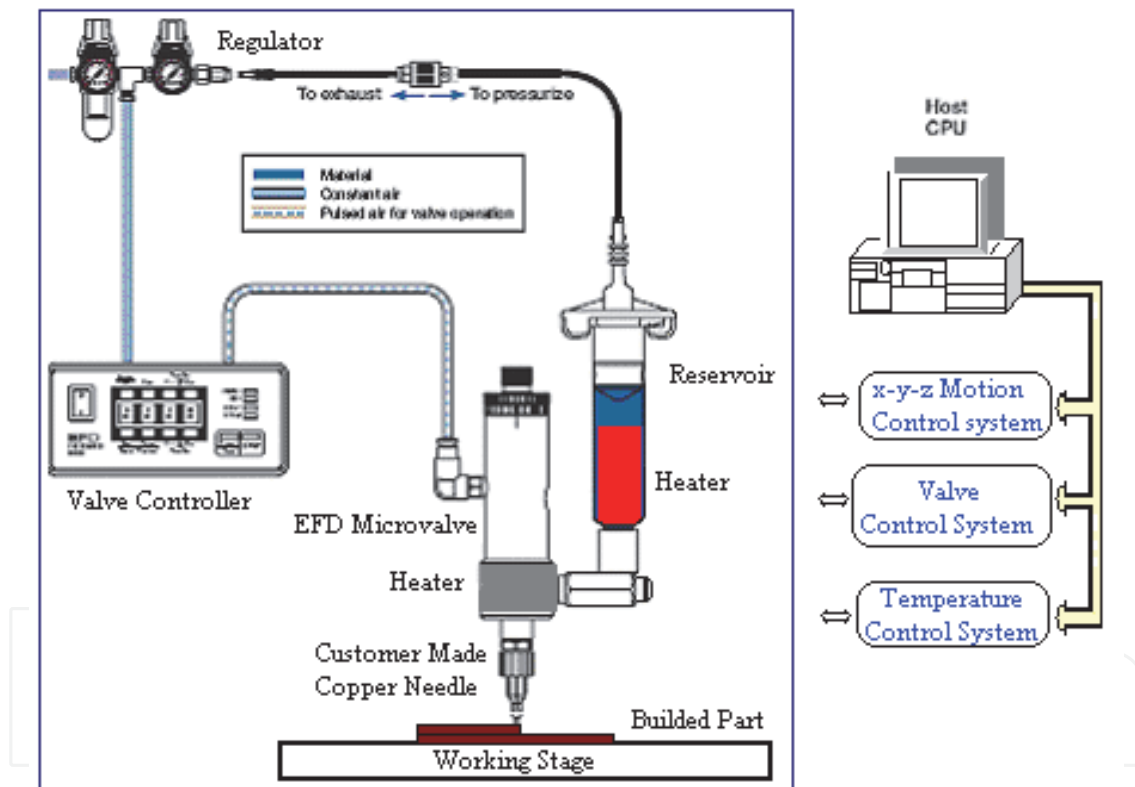
Fig. 29. Component Diagram of designed SFF system.

4.3 Scaffold and structured porogen design for the sucrose SFF machine

In order to test the machinability of our SFF machine a scaffold was designed with fully interconnected voids to enable the injection of scaffold material with a syringe. By using a syringe, a pressure could be applied to the scaffold material to help overcome the frictional forces resisting material flow through the porogen. Three-dimensional models of the scaffolds and corresponding porogens were created using Pro/Engineer and saved as STL files required by the fabrication system.

4.4 Fabrication of scaffolds

The designed porogen structures have been fabricated based on the CAD design similar to Figure 24 F. The designed distance between each strut from center to center is 1000µm. The target strut diameter is 500µm, therefore the spacing between strut is 500µm in both horizontal and vertical direction. Based on our design of experiment results, a motor speed of 0.1m/s, pressure of the controller of 30 psi, pressure of the reservoir of 90psi and temperature of 90°C were set to fabricate the designed porogen. A sucrose porogen with approximately 600µm struts and 400µm spacing between the struts can be made using this SFF machine. If 20 layers of sucrose mixture were printed on the platform, then it takes about 30 minutes to complete the whole porogen. Since the sucrose mixture solidified right after it attached to the substrate at room temperature, there is no external cooling needed. The fabricated porogen was stored in a sealed Petri dish and placed into the freezer waiting for the injection.

Following the fabrication of sucrose porogen, PCL scaffolds were fabricated as described in previous sections. Briefly, the PCL and porogen were first placed in an oven at a temperature of 70° C. During heating the PCL was occasionally agitated manually and visually inspected for solid particles. After one hour the PCL and porogen were removed from the oven. The molten PCL was then quickly packed into a syringe and injected into the porogen by inserted the needle into the bottom of the porogen. Excess PCL was removed with a spatula. The PCL was then allowed to cool to room temperature. Once at room temperature, the filled porogen was placed in DI water to separate the sucrose porogen material from the PCL. The DI water in the water bath was removed and replenished with new water for a minimum of three times. The PCL scaffold was then allowed to air-dry at room temperature.

Followed by the removal of sucrose porogen, PCL scaffolds can be obtained. The smallest strut size on the scaffold is about 250µm and the porogen diameter varies from 250µm - 500µm.

4.5 Biocompatibility

As we expected that the sucrose porogen made scaffold give us a much better biocompitability. To prove this, the following biocompatibility test has been done using the same methods as the 3DP scaffolds (section 2.5.2). Briefly, the scaffolds have been washed thoroughly and sterilized with 70% ethanol for 30 minutes twice at room temperature, and washed 3 times with sterile PBS. After that the scaffolds have been air dried in the hood for two hours. The dried scaffolds were then incubated with 10µg/ml Fibronectin in DMEM overnight at 37°C on an orbital shaker. Scaffolds were then seeded with a suspension of 0.5 million EAhy 926 cells/ml for three hours on an orbital shaker. Following seeding and after 48 hours culture, the samples were fixed in 10% buffered formalin for 15 minutes at room temperature. Then the scaffolds were washed using PBS for three times. Then the samples were washed once more with PBS and incubated with PBS containing 2µg/mL Hoechst 33258 a nuclear stain and rhodamine phalloidin for 30 minutes. After that the samples were washed using PBS for three times.

The microscope images show the cell growing after 48 hours post-seeding in Figure 30. Figure 30A shows the nuclei of EAhy 926 cells cultured on sucrose molded PCL scaffolds. We noticed that the cell attached to the scaffold. Figure 30B shows an overlay of bisbenzimide and rhodamine phalloidin staining of EAhy 926 cells cultured on sucrose

molded PCL scaffold. Figure 30C shows the cells are confluent. Staining for nuclei and cytoskeletal filaments of EAhy 926 cells seeded onto sucrose-molded PCL scaffolds demonstrated cell attachment and growth over a 48 hour culture period.


| (A) | (B) | (C) |
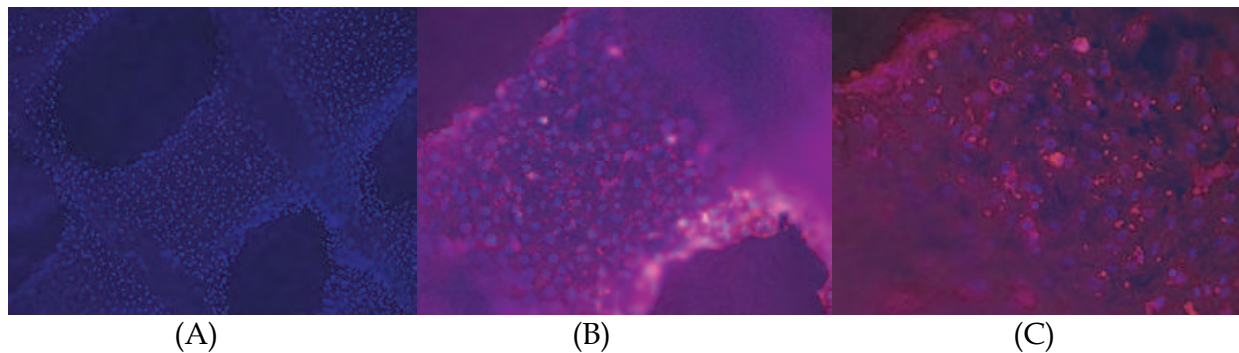
Fig. 30. Fluorescent stains of cells growing on PCL scaffolds. (A) Bisbenzimide stain showing nuclei of EAhy 926 cells cultured on sucrose molded PCL scaffolds after 48 hours post-seeding, 5× (B) Overlay of bisbenzimide and rhodamine phalloidin staining of EAhy 926 cells cultured on PCL scaffolds for 48 hours, 10X (C) Cells are confluent on the sucrose molded PCL scaffold after 48 hours of seeding, 20X.

The biocompatibility of the scaffolds was also assessed using Osteoblast cell line. Briefly, 7F2 cells were seeded on the scaffolds coated with 20μg/ml collagen type I with a suspension of 1 million 7F2 cells/ml for 3 hours on an orbital shaker (Belly Dancer, Stovall). Following seeding, the initial level of cell seeding was assessed by the Alamar Blue™ (Biosource) assay. In order to evaluate cell growth on the PCL scaffolds the Alamar Blue™ assay was performed again on the same samples at day 2, 4 and 6 post-seeding. Subsequently, the samples were fixed in 10% neutral buffered formalin (Fisher Scientific) for 1 hour at room temperature and stored in PBS at 4°C until cytological staining. For staining, the samples were washed once more with PBS and incubated with PBS containing 2μg/mL Hoechst 33258 (Bisbenzimide, Sigma), a nuclear stain and 1μg/mL rhodamine phalloidin, a cytoskeleton stain.

The results show that 7F2 cells were able to attach to the PCL scaffolds as evidenced by fluorescent staining with Hoechst 33258 and rhodamine phalloidin (Figure 31A). Figure 31B shows that osteoblasts grew well and they were confluent after 4 days of post seeding on PCL scaffolds. The morphology of 7F2 cells growing on PCL scaffolds was examined by SEM (Figure 32). As seen in Figure 32A the cells flatten on the surface. We note that after 4 days post-seeding cells were everywhere over the whole surface. Metabolic activity measured by Alamar Blue™ revealed growth of osteoblasts on PCL scaffolds. The result indicate the continuous growing and proliferation of the 7F2 cells on the PCL scaffolds. The comparison of Alamar Blue metabolic activity results for sucrose molded PCL scaffolds and Plaster molded PCL/CaP scaffolds has shown that the metabolic activity on sucrose molded PCL scaffolds grew much faster than on plaster molded PCL scaffolds and even can be faster than that on PCL/CaP composite scaffolds which proves that the residues of sucrose do not have effect on cellular function and the environment is benign. This further confirms that it is necessary to design a SFF machine which can print biocompatible porogen materials.
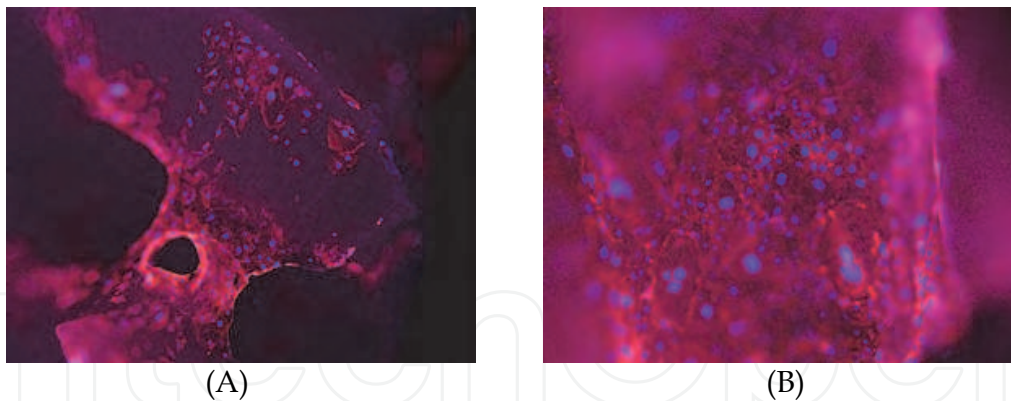
Fig. 31. Overlay of bisbenzimide and rhodamine phalloidin staining of 7F2 cells cultured on PCL scaffolds (A) day 2, showed the initial attachment, 5X (B) day 4, showed the cells were confluent, 10X.
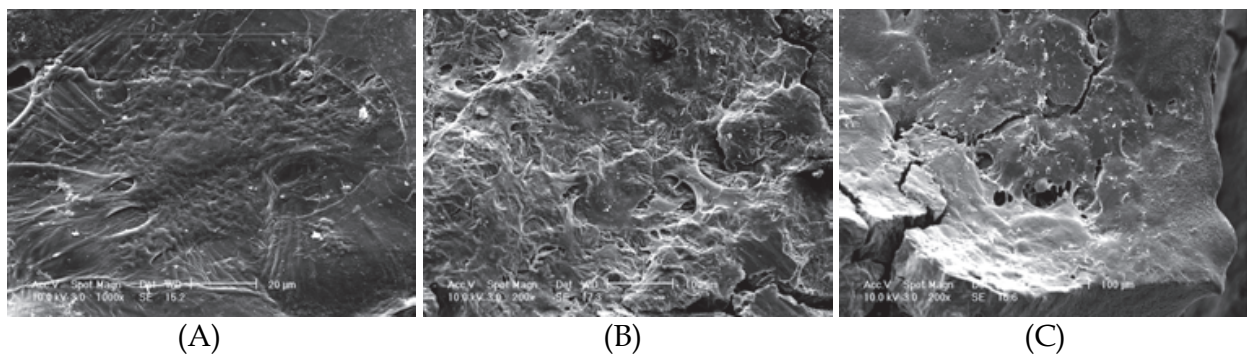

Fig. 32. SEM images of 7F2 growing onto the PCL scaffolds (A) Flattened 7F2 cells on PCL scaffold, Scale bar = 20 µm (B) day 1 (C) day 4.

5. Conclusion

This study developed a structured porogen-based fabrication method using the DDP, 3-DP and custom-designed SFF manufacturing systems. By indirect building, the resolution of our fabricated scaffolds can be improved at least 3-fold as compared to directly built scaffolds made by the same kind of SFF machine. This fabrication method gave us the ability to use multiple biomaterials for injection molding with a single ubiquitous porogen. By using the bio-composite material of calcium phosphate and Poly (ε-caprolactone), the mechanical strength and bioactivity have been improved dramatically. The structured porogen-based fabrication method also provided the ability to make complex structures which has the exact shape and similar predefined internal structure of the bone tissue with sufficient mechanical strength. A new custom designed SFF system has been developed. By combining this novel fabrication method with new bio-composite materials, the bone manufacturing technology can be highly advanced.

This research will help to build knowledge and lead to novel solutions in fabricating polymeric scaffolds in bone tissue engineering applications. This research has the potential to advance scientific knowledge, enhance our manufacturing industry competitiveness and benefit our nation's health and economy. More specifically, this research involves both fundamental scientific research and experimental engineering studies. Research on new bio-

composite materials, new SFF system design and integration and system control of the machine has been conducted. The notion of combining materials to form a composite scaffold has been investigated extensively, There has not been, however, a similar methodology to the one described in this manuscript for bone scaffolds fabrication.

6. Acknowledgement

7. References

Albee FH. 1920. *Annual Surgery* 71: 33-7

Athanasiou KA, Zhu L, Wang X. 2000. *Tissue Engineering* 6: 361-81

Barralet JE, Grover L, Gaunt T, Wright AJ, Gibson IR. 2002. *Biomaterials* 23: 3063-72

Bock RG, Goode AJ, Novartis F. 2003. *Tissue engineering of cartilage and bone*: John Wiley and Sons. 133-47

Burg JLK, Porter S, Kellam FJ. 2000. *Biomaterials* 21: 2347-59

Carter DR, Hayes WC. 1976. *Science* 194: 1174-6

Chapekar SM. 2000. *Journal of Biomedical Materials Research* 53: 617-20

Chen DR, Bei JZ, Wang SG. 2000. *Polymer Degradation and Stability* 67: 455-9

Coelho MdB, Pereira MM. 2005. *Journal of Biomedical Materials Research Part B: Applied Biomaterials* 75B: 451-6

Coombes AGA, Heckman JD. 1992. *Biomaterials* 13: 217-24, 97-307

Cuckler MJ. 2004. *The Journal of Arthroplasty* 19 56-8

Cutter CS, Babak JM. 2006. *Journal of Long-Term Effects of Medical Implants* 16: 249-60

Darling AL, Sun W. 2004. *Journal of biomedical materials research. Part B Applied Biomaterials* 70B: 311-7

de Groot K. 1984. In *Biocompatibility of clinical implant materials*, ed. W DF, pp. 199-222: Boca Raton, FL: CRC Press

Freyman TM, Yannas IV, Gibson LJ. 2001. *Progress in Materials Science* 46: 273-82

Gadzag AR, Lane JM, Glaster D, Forster RA. 1995. *Journal of the American Academy of Orthopaedic Surgeons* 3: 1-8

Geiger M. 2001. *Porous Collagen/Ceramic Composite Carriers for Bone Regeneration Using Recombinant Human Bone Morphogenetic Protein-2 (rhBMP-2)*. University of Erlangen-Nuremberg, Erlangen, Germany. 5 pp.

Geng L, Feng W, Hutmacher DW, Wong YS, Loh HT, Fuh JYH. 2005. *Rapid Prototyping Journal* 11: 90-7

Giannoudis VP, Dinopoulos H, Tsiridis E. 2005. *Injury* 36: S20-S7

Harris DL, Kim B-S, Mooney JD. 1998. *Journal of Biomedical Materials Research* 42: 396-402

Hollister SJ, Maddox RD, Taboas JM. 2002. *Biomaterials* 23: 4095-103

Hutmacher W, Schantz T, Zein I, Ng K, Teoh S, Tan K. 2001. *Journal of biomedical materials research. Part B, Applied biomaterials* 55: 203–16

Hutmacher WD. 2000. *Biomaterials* 21: 2529-43

Kelly BE. 2000. *Orthopedic Technology Review* 2: 28-34

Kim H-W, Knowles JC, Kim H-E. 2003. *Biomaterials* 25: 1279-87

Klawitter JJ, Hulbert SF. 1971. *Journal of Biomedical Materials Research Symposium* 2: 161

Langer R, Vacanti J. 1993. *Science* 260: 920-6

Laurencin CT, Ambrosio AMA. 1999. *Annual Review of Biomedical Engineering* 1: 19-46

Lee JH, Ryu H-S, Lee D-S, Hong KS, Chang B-S, Lee C-K. 2005. *Biomaterials* 26: 3249–57

LeGeros RZ, Parsons JR, Decals G, Driessen F, Lee D, et al. 1988. *Annals of the New York Academy of Sciences* 523: 268-71

Li M, Mondrinos M, Gandhi M, Ko F, Weiss A, Lelkes P. 2005. *Biomaterials* 26: 5999-6008

Li W-J, Tuli R, Okafor C, Derfoul A, Danielson GK, et al. 2005. *Biomaterials* 26

Ma J, Wang H, He B, Chen J. 2001. *Biomaterials* 22: 331-6

Mehta S. 1995. *Analysis of the mechanical properties of bone material using nondestructive ultrasound reflectometry.* University of Texas Dallas

Mikos A, Bao Y, Cima L, Ingber D, Vacanti J. 1993. *Journal of Biomedical Materials Research* 27: 183-9

Misch CE, Qu Z, Bidez MW. 1999. *Journal of Oral & Maxillofacial Surgery* 57: 700-6

Mistry A, Mikos A. 2005. *Advances in Biochemical Engineering/Biotechnology* 94: 1-22

Mooney DJ, Baldwin DF, Suh NP, Vacanti JP, Langer R. 1996. *Biomaterials* 17: 1417-22

Ohgushi H, Miyake J, Tateishi T. 2003. *Mesenchymal stem cells and bioceramics: strategies to regenerate the skeleton.*: Novartis Foundation. 118-27.

Ren J, Ren T, Zhao P, Huang Y, Pan K. 2007. *Journal of Biomaterials Science, Polymer Edition* 18: 505-17

Rho J-Y, Liisa K-S, Zioupos P. 1998. *Medical Engineering & Physics* 20: 92–102

Rohner DW, Hutmacher TK, Cheng M, Oberholzer, Hammer M. 2003. *Journal of Biomedical Materials Research: Applied Biomaterials* 66B: 574-80

Ruhe PQ, Hedberg EL, Padron NT, Spauwen PH, Jansen JA, Mikos AG. 2003. *The Journal of Bone and Joint Surgery* 85-A: 75-81

Ruhe PQ, Hedberg EL, Padron NT, Spauwen PH, Jansen JA, Mikos AG. 2005. *Journal of Biomedical Materials Research: Applied Biomaterials* 74: 533-44

Saito N, Takaoka K. 2003. *Biomaterials* 24: 2287-93

Shin M, Yoshimoto H, Vacanti JP. 2004. *Tissue Engineering* 10: 33-41

Silber J, Anderson D, Daffner S. 2003. *Spine* 28: 134-9

Singhal A, Agrawal C, Athannasiou K. 1996. *Tissue Engineering* 2: 197-207

Taboas JM, Maddox RD, Krebsbach PH, Hollister SJ. 2003. *Biomaterials* 24: 181-94

Thomson R, Mikos A, Beahm E, Lemon JC, , Satterfield W, Aufdemorte T, Miller M. 1999. *Biomaterials* 20: 2007-18

Wang T, Tian WD, Liu L, Cheng XZ, Liao YM, Lin SW. 2005. *Hua Xi Kou Qiang Yi Xue Za Zhi* 23: 106-9

Weiner S, Traub W. 1992. *Journal of the Federation of American Societies for Experimental Biology* 6: 879-85

Weiner S, Wagner HD. 1998. *Annual Review of Materials Research* 28: 271-98

Williams JM, Adewunmi A, Schek RM, Flanagan CL, Krebsbach PH, Feinberg SE. 2005. *Biomaterials* 26: 4817-27

Xu HH, Quinn JB, Takagi S, Chow LC. 2004. *Biomaterials* 25: 1029-37

Xu HH, Simon CGJ. 2004. *Journal of Orthopaedic Research* 22: 535-43

Xu HH, Simon CGJ. 2005. *Biomaterials* 26: 1337-48

Yang C, Hillas PJ, Baez JA, Nokelainen M, Balan J, et al. 2004. *Tissue Engineering* 18: 103-19

Yudkin J, Edelman J, Hough L. 1971. *Sugar - Chemical, Biological and Nutritional Aspects of Sucrose*. London: The Butterworth Group

Zein I, Hutmacher DW, Tan KC, Teoh SH. 2002. *Biomaterials* 23: 1169–85
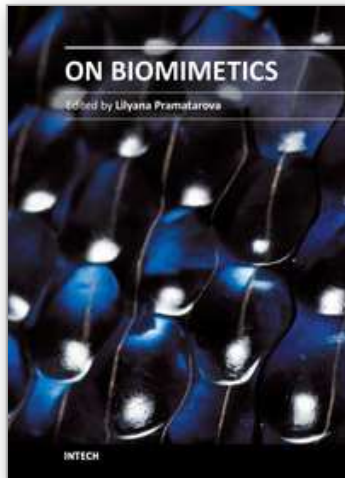
On Biomimetics

Edited by Dr. Lilyana Pramatarova

Bio-mimicry is fundamental idea â€˜How to mimic the Natureâ€™ by various methodologies as well as new ideas or suggestions on the creation of novel materials and functions. This book comprises seven sections on various perspectives of bio-mimicry in our life; Section 1 gives an overview of modeling of biomimetic materials; Section 2 presents a processing and design of biomaterials; Section 3 presents various aspects of design and application of biomimetic polymers and composites are discussed; Section 4 presents a general characterization of biomaterials; Section 5 proposes new examples for biomimetic systems; Section 6 summarizes chapters, concerning cells behavior through mimicry; Section 7 presents various applications of biomimetic materials are presented. Aimed at physicists, chemists and biologists interested in biomineralization, biochemistry, kinetics, solution chemistry. This book is also relevant to engineers and doctors interested in research and construction of biomimetic systems.

How to reference

In order to correctly reference this scholarly work, feel free to copy and paste the following:

INTECH
open science | open minds